Towards robust dosimetry for diffusing alpha-emitters radiotherapy

Victor Daniel Diaz Martinez

Medical Physics Unit
McGill University
Montréal, Québec, Canada

March 2023

A thesis submitted to McGill University in partial fulfillment of the requirements of the degree of master of science in medical radiation physics

Contents

1 Introduction **8**

1.1 Rationale, Objectives, and Outline 8

2 Literature Review **10**

2.1 Ionizing Radiation 10

2.1.1 Interactions of Radiation with Matter 10

2.1.2 Linear Energy Transfer (LET) and RBE 12

2.2 Radiation Therapy 14

2.2.1 External Beam Radiotherapy 14

2.2.2 Brachytherapy 15

2.2.3 Radioactive Decay 15

2.2.4 Effects of α-particles in tissue 17

2.2.5 Diffusing Alpha-emitters Radiation Therapy (DaRT) in Brachytherapy 18

2.2.6 Seed Preparation and ^{224}Ra Decay Chain 19

2.3 Dosimetry and Radiation Detection 22

2.3.1 TG-43 22

2.3.2 Alpha Particle Dosimetry using Radiochromic Films 22

2.4 Monte Carlo Method 24

2.4.1 Geant4 Simulation Toolkit 25

3 Body of Thesis **26**

3.1 Introduction 28

3.2 Methods 30

3.2.1 Unlaminated EBT3 Model GafChromic® Film and Source Characteristics 30
3.2.2 Monte Carlo Simulations . . . 32
3.3 Results . . . 36
3.3.1 Monte Carlo Simulations . . . 36
3.3.2 Film Irradiations . . . 38
3.4 Discussion . . . 40
3.4.1 Monte Carlo Simulations . . . 41
3.4.2 Film Irradiations . . . 42
3.5 Conclusion . . . 46
3.6 References . . . 46
3.7 Author contributions statement . . . 50
3.8 Additional information . . . 51

4 Body of Thesis 53
4.1 Introduction . . . 55
4.1.1 Diffusing alpha-emitters Radiation Therapy Technology . . . 55
4.1.2 Monte Carlo Method . . . 58
4.1.3 Aim . . . 58
4.2 Methods . . . 59
4.2.1 DaRT source characteristics . . . 59
4.2.2 Monte Carlo Simulations . . . 59
4.3 Results . . . 63
4.3.1 Energy Spectra emitted from the ^{224}Ra source . . . 63
4.3.2 The Positioning method results . . . 64
4.4 Discussion . . . 66
4.5 Conclusion . . . 69
4.6 References . . . 69
4.7 Author contributions statement . . . 73
4.8 Additional information . . . 73

5 Discussion 74

6 Conclusion and Future Work **82**

List of Figures

2.1 Curtain plot 12
2.2 Relative Biological Effectiveness 14
2.3 Scheme of the decay chain of ^{224}Ra 21
2.4 H&D curve 23
2.5 Scheme of the EBT3 film 24

3.1 Components and thicknesses of the laminated and unlaminated EBT3 model GafChromic® film 31
3.2 Picture and diagram of the ^{241}Am disk source 31
3.3 Experimental setup for film irradiation 35
3.4 Energy Spectra of the ^{241}Am source 38
3.5 Dose rate per voxel, dose rate profile, and ROI 38
3.6 Film response of the unlaminated EBT3 model GafChromic® film 39
3.7 Normalized pixel values and uncertainties with no high doses 40

4.1 Scheme of ^{224}Ra Decay Chain 57
4.2 Geometry of the seeds and representation of the mechanism of the DaRT technology 59
4.3 Workflow of the *'positioning method'* 62
4.4 Alpha, beta, and photon energy spectra emitted from the ^{224}Ra decay 64
4.5 Visualization of the positioning method 65
4.6 Dose maps of the DaRT seed as a function of the distance 66

List of Tables

2.1 Classification of ionizing radiation 11
2.2 Description of Low and High LET 12
2.3 Most common radionuclides used in brachytherapy 15

3.1 Composition and characteristics of the unlaminated EBT3 model GafChromic® film 31
3.2 Summary of parameters used for Monte Carlo simulation 33
3.3 PV_{norm} results for the exposure batches 40
3.4 Comparison of MC input parameters 43

4.1 Most common radionuclides used in brachytherapy 56
4.2 Summary of parameters used for Monte Carlo simulation 61

Glossary

^{212}Pb Lead 212.

^{220}Rn Radon 220.

^{224}Ra Radium 224.

DaRT Diffusing Alpha-emitters Radiation Therapy.

LET Linear Energy Transfer.

MC Monte Carlo.

Abstract

A novel brachytherapy technique that uses α-emitting radionuclides, known as Diffusing alpha-emitters Radiation Therapy (DaRT), was recently introduced to treat solid tumors. DaRT consists of ^{224}Ra atoms fixed on the surface of a metallic seed that α-decay into short-lived α-particle emitting atoms that diffuse between the tumor cells. Although the range of the emitted α-particles is a couple of cell diameters, the diffusing atoms (^{220}Rn and ^{212}Pb) contribute to a high-dose region that extends up to a few millimeters around the source. Currently, there is a lack of robust α-based dosimetry protocols for DaRT based on film dosimetry, development of radiation detectors, and simulation toolkits for benchmarking. External beam radiotherapy (EBT) Gafchromic® films have been widely used in radiation therapy for photon-dosimetry purposes. However, only a few published papers have adapted the photon-film dosimetry to α-particles and have benchmarked their results with Monte Carlo (MC) simulations. In addition, there is a lack of detectors for DaRT acceptance testing, quality assurance, and in *in-vivo* dosimetry. Both applications can be studied in detail through MC simulations.

In this thesis, an MC-based toolkit was developed to be used for film dosimetry and detector development applications. The response of the unlaminated GafChromic® EBT3 film to α-radiation was studied, as well as the dose distribution from DaRT seeds due to the environmental diffusion of the diffusing radionuclides. In this MC-based toolkit, the geometry and materials of the radiation sources and radiochromic film were modeled in detail according to the vendor's specifications. All the physics processes of the α-emitting radionuclides were simulated in detail and the absorbed dose was scored in voxelized geometries.

For both simulations, the results were found to be in good agreement with published reported values. From the film dosimetry simulations, the energy spectra of the α-emitting

source were found to be in good agreement with the IAEA database (0.036-0.516% and 0.001-0.006% difference ranges for α-particles and γ-photons, respectively). A dose rate value was obtained for the active layer material of the unlaminated GafChromic® EBT3 film using the ^{241}Am source, which had a value of 1.09 $\pm$ 0.04 Gy/min. Experimental measurements were performed to irradiate this film using the simulated dose rate value and to obtain the average net optical densities and normalized pixel values per RGB channel. The results showed that an exponential fit to each channel is promising for α-film dosimetry compared to other fits used. From the DaRT seed simulations, the energy spectra obtained from the ^{224}Ra decay were also in good agreement with reported values within acceptable percentage difference ranges (0.006-0.015% for α-particles, 4.812%, 0.179%, and 0.240% for the three β-particles energy spectra, and 0-0.081% for γ-photons). The diffusion of ^{220}Rn and ^{212}Pb allowed the α-particles to extend $\sim$3-4 mm contributing to the dose around the seed.

In this work, an MC-based toolkit was developed for α-based dosimetry purposes, which can be used to benchmark dosimetry protocols for any type of α-emitting sources combined with detectors such as radiochromic films or the development of quality assurance (QA) and *in-vivo* detectors destined for DaRT.

Abrégé

La curiethérapie, en particulier sous guidage IRM, est l'une des modalités d'irradiation les plus efficaces et les plus précises pour certains types de tumeurs dans le traitement du cancer. Une nouvelle technique de curiethérapie utilisant des radionucléides émetteurs α, connue sous le nom de radiothérapie par émetteurs alpha diffusants (DaRT), a été récemment introduite pour traiter les tumeurs solides. La DaRT consiste à fixer des atomes de ^{224}Ra à la surface d'une graine métallique qui se désintègrent en atomes émetteurs de particules α de courte durée qui se diffusent entre les cellules tumorales. Bien que la portée des particules α émises soit de quelques diamètres de cellules, les atomes diffusants (^{220}Rn et ^{212}Pb) contribuent à une région à forte dose qui s'étend jusqu'à quelques millimètres autour de la source. À l'heure actuelle, il n'existe pas de protocoles de dosimétrie α robustes pour la DaRT, basés sur la dosimétrie sur film, le développement de détecteurs de rayonnement et des outils de simulation pour l'évaluation comparative. Les films Gafchromic® de radiothérapie externe (EBT) ont été largement utilisés en radiothérapie à des fins de dosimétrie photonique. Cependant, seuls quelques articles publiés ont adapté la dosimétrie des films photoniques aux particules α et ont comparé leurs résultats avec des simulations de Monte Carlo (MC). En outre, il y a un manque de détecteurs pour les tests d'acceptation DaRT, l'assurance qualité et la dosimétrie in vivo. Ces deux applications peuvent être étudiées en détail grâce aux simulations MC.

Dans cette thèse, une boîte à outils basée sur la MC a été développée pour être utilisée dans les applications de dosimétrie des films et de développement des détecteurs. La réponse du film GafChromic® EBT3 non laminé au rayonnement α a été étudiée, ainsi que la distribution de la dose des semences DaRT due à la diffusion environnementale des radionucléides diffusants. Dans cette boîte à outils basée sur MC, la géométrie et les

matériaux des sources de rayonnement et du film radiochromique ont été modélisés en détail conformément aux spécifications du fournisseur. Tous les processus physiques des radionucléides émetteurs α ont été simulés en détail et la dose absorbée a été évaluée dans des géométries voxélisées.

Pour les deux simulations, les résultats se sont avérés être en bon accord avec les valeurs rapportées dans la littérature et ont été comparés aux travaux publiés. Les simulations de dosimétrie sur film ont montré que les spectres de la source émettrice α étaient en bon accord avec la base de données de l'AIEA (0,036-0,516% et 0,001-0,006% de différences pour les particules α et les photons γ, respectivement). Une valeur de débit de dose de 1,06 $\pm$ 0,04 Gy/min a été obtenue pour le matériau de la couche active du film GafChromic® EBT3 non laminé. Des mesures expérimentales ont été effectuées pour irradier ce film en utilisant le débit de dose simulé et pour obtenir les densités optiques nettes moyennes et les valeurs normalisées des pixels par canal RVB. Les résultats ont montré qu'un ajustement exponentiel à chaque canal est prometteur pour la dosimétrie des films α par rapport aux autres ajustements utilisés. D'après les simulations de semences DaRT, les spectres obtenus à partir de la désintégration du ^{224}Ra étaient également en bon accord avec les valeurs rapportées dans des plages de différences de pourcentage acceptables (0,006-0,015% pour les particules α, 4,812%, 0,179% et 0,240% pour les trois spectres β, et 0-0,081% pour les photons γ). La diffusion du ^{220}Rn et du ^{212}Pb a permis aux particules α de s'étendre jusqu'à $\sim$3-4 mm, contribuant ainsi à la dose autour de la graine.

Dans ce travail, une boîte à outils basée sur la MC a été développée à des fins de dosimétrie basée sur l'α, qui peut être utilisée pour comparer les protocoles de dosimétrie pour tout type de sources émettant de l'α combinées avec des détecteurs tels que des films radiochromiques ou le développement de l'assurance qualité (AQ) et des détecteurs in-vivo destinés à la DaRT.

Acknowledgements

'Me has hecho conocer los caminos de la vida; me llenarás de gozo con tu prescencia.' Hechos 2:28

First, I thank ***God*** for always being by my side since I was a child. I thank Him because my life has found grace in His eyes and because He gave the opportunity to study a degree in Canada. To my ***parents***, thank you for all your support, concern, and teachings which good or bad, have shaped my life and I am still learning from you. ***Abigail***. Thank you for coming into my life when I needed it the most, thank you for being with me in the distance, for always pushing me to be a better student, and for always motivating me to seek God. You will always be part of me. Do not forget me. To my ***dear old friends*** Brian, Erick, Francisco, Alex, and Saret, thank you for your unconditional friendship, love, and support over the years. My colleagues from my cohort, and all the members at the EngerLab for their help provided through this project.

Dr. Shirin A. Enger. Thank you for all your guidance and support during this project, thank you for trusting me. I personally thank you for your understanding and concern with regard to the difficult situation that I was facing. I thank McGill University and the Medical Physics Unit for letting me be part of this great group of professionals. I thank the Consejo Nacional de Ciencia y Tecnología (CONACyT), Mexico for being granted the 'CONACyT-Regional Centro 2020' scholarship to study in Canada. I would also like to thank all the funding agencies including the Institut TransMedTech Montreal, AlphaTau Medical, and the Jewish General Hospital Foundation. Special thanks to the Cedar cluster of the Digital Research Alliance of Canada for providing computational resources.

Contribution of Authors

The body of this thesis contains two main manuscripts presented in chapter 3 (both under preparation): '*Investigation of dosimetric characteristics of GafChromic® EBT3 film for alpha particle radiation*', and '^{220}*Rn and* ^{212}*Pb distribution from radioactive seeds in Diffusing alpha-emitters Radiation Therapy (DaRT)*'.

Investigation of dosimetric characteristics of GafChromic® EBT3 film for alpha particle radiation

In this first manuscript, the co-first authorship is shared with my colleague Mélodie Cyr. According to the graduate and postdoctoral studies regulations, this manuscript will only be included in my thesis. As a co-first author to this manuscript, I developed, performed, and analyzed the results obtained from the Monte Carlo simulations. These results were used by Mélodie Cyr. Mélodie performed and analyze the experimental measurements. The contributions of the co-authors were, respectively: Dr. Devic Slobodan shared his expertise in EBT photon-based film dosimetry, besides useful comments regarding the manuscript, Nada Tomic helped Mélodie and myself with the film measurements. Dr. David F. Lewis provided accurate dimensions and composition of the GafChromic® EBT3 films and shared his experience on radiochromic film dosimetry, and finally my supervisor Dr. Shirin A. Enger; provided a preliminary version of the Geant4 user-code which I later modified according to the needs of the experiment, and providing continuous and valuable feedback on this manuscript.

This work was presented at the following conferences:

1. Mélodie Cyr, Victor D. Diaz-Martinez, Slobodan Devic, Nada Tomic, David Lewis, and Shirin Enger.Investigation of dosimetric characteristics of GafChromic® EBT3 Film Response to Alpha Particle Irradiation. IC3DDose Annual Meeting. Quebec City,

June 19-23, 2022 (Oral Presentation).

2. Victor D. Diaz-Martinez, Mélodie Cyr, Slobodan Devic, Nada Tomic, David Lewis, and Shirin Enger. '*Use of the Monte Carlo Method to Relate Radiochromic Film Response to Absorbed Dose for Alpha Particle Dosimetry*'. COMP Annual Scientific Meeting. Quebec City, June 22-25, 2022 (Poster).

^{220}Rn and ^{212}Pb distribution from radioactive seeds in Diffusing alpha-emitters Radiation Therapy (DaRT)

As the first author in this second manuscript, I developed, performed, and analyzed the results obtained from the Monte Carlo simulations. The contribution of the co-authors was, respectively: Liam Carroll provided useful and valuable ideas for implementation of the Monte Carlo-based dose calculation software, Dr. Devic Slobodan provided useful comments with regards to this manuscript, and my supervisor Dr. Shirin A. Enger provided continuous and valuable ideas and feedback on this manuscript.

This work was accepted at the following conference:

1. Victor D. Diaz-Martinez, Liam Carroll, and Shirin Enger. '*^{220}Rn distribution from radioactive seeds in Diffusing alpha-emitters Radiation Therapy (DaRT)*'. AAPM Annual Scientific Meeting. Washington DC, July 10-14, 2022 (ePoster).

Chapter 1

Introduction

1.1 Rationale, Objectives, and Outline

According to statistics reported by the Canadian Cancer Society, cancer is the main cause of death, representing 28.2% of all deaths in Canada. The most commonly diagnosed cancers that account for 46% of all new cancer cases include lung, breast, colorectal, and prostate cancer. Each type of cancer represents 13%, 25%, 10%, and 20% of all new cases, respectively [1]. Radiotherapy is an effective and safe treatment for cancer. Approximately 50% of patients diagnosed with cancer benefit from this treatment, which is close to 100,000 Canadians with cancer each year. New technology developments in external beam radiotherapy during the last decades have led to improvements in tailoring the radiation dose to the shape of the tumor and minimizing the dose to organs at risk. However, the location of the tumor within the organ, errors in treatment delivery such as incorrect patient positioning, tumor/patient movement during the treatment, and the use of large margins result in the use of large treatment fields to account for uncertainties in the tumor and organs at risk. Brachytherapy is a type of radiotherapy, where encapsulated radiation sources are placed permanently or temporarily, directly into or near localized tumors, giving a high radiation dose to the malign volume while the dose to more distant healthy tissues is lower. The majority of the sources used in brachytherapy are photon emitters with low linear energy transfer (LET).

Image-guided brachytherapy treatment planning has enabled improved tumor delineation

and indicated the need for brachytherapy dose delivery techniques with increased tumor dose conformity. However, the dose distribution from conventional brachytherapy sources often results in less than ideal tumor dose conformity due to the non-symmetrical shape of the tumors resulting in dose spillage to radiation-sensitive healthy tissues, hence despite existing evidence of its efficacy, there are still much toxicities related to conventional brachytherapy.

Recently a novel brachytherapy treatment option for solid tumors is being offered through alpha emitters released from ^{224}Ra-loaded brachytherapy seeds. This novel technique is called diffusing alpha-emitters radiotherapy (DaRT), where ^{224}Ra atoms undergo α-decay, releasing high-energy α-particles, ^{220}Rn, and several other radioactive daughters, that diffuse through the tumor volume undergoing radioactive decay. This way, a lethal dose of radiation is delivered to the tumor while sparing nearby radiation-sensitive healthy tissues due to the short range of α-particles in tissue. However, due to the lack of robust dosimetry protocols for this technique, new dosimetry standards are required. Such standards include film dosimetry and detector development for DaRT.

The main objective of this thesis was to develop a Monte Carlo-based (MC) software package to study the response of unlaminated GafChromic® EBT3 film to α-radiation. This information was used to develop a dose-calibration protocol. The software package was also used to study the dose distribution of DaRT seeds due to the diffusive daughters.

This thesis is divided into five chapters. Chapter 1 is a short introduction to the topic and states the main objectives of this thesis. Chapter 2 focuses on the background and literature review needed for the scope of this thesis. This chapter includes a review of ionizing radiation, the interaction of radiation with matter, radiotherapy techniques such as external beam radiotherapy and brachytherapy, dosimetry in brachytherapy, published work on α-based film dosimetry and DaRT, and a review of the MC method. The body of the thesis is stated in chapters 3 and 4, which contain the manuscripts for film dosimetry and diffusion in DaRT, respectively. In Chapter 5, the MC results obtained for both manuscripts are discussed and compared to published results to benchmark the developed user code. Chapter 6 summarizes, and concludes the findings of this thesis and offers insight into future work.

Chapter 2

Literature Review

2.1 Ionizing Radiation

Radiation has been defined as energy in motion in the form of electromagnetic radiation or particles through space or matter, also referred to as the absorber [2]. Radiation is classified as ***ionizing*** or ***non-ionizing***, where ionizing radiation is one of special interest in radiation therapy. Ionizing radiation has been defined as radiation with sufficient energy to ionize atoms and molecules by ejecting electrons [3]. Depending on the type of particle, ionizing radiation has been further classified as ***directly*** and ***indirectly ionizing radiation***.

Directly ionizing radiation is produced by charged particles that deposit their energy through Coulomb interactions between the charged particle and the orbital electrons [3]. With indirectly ionizing radiation, non-charged (neutral) particles release electrons from the absorber through different interactions, and these electrons deposit their energy through Coulomb interactions. Table 2.1 entails examples of the type of particles involved in directly and indirectly ionizing radiation.

2.1.1 Interactions of Radiation with Matter

Ionization can be produced by charged or non-charged particles, therefore they will have different types of interactions.

Ionizing Radiation	Examples
Directly	α-particles electrons protons heavy ions
Indirectly	x-rays γ-rays neutrons

Table 2.1: Classification of ionizing radiation as directly and indirectly ionizing radiation showing examples of the type of particles involved.

Interactions of Charged Particles with Matter

As stated before, charged particles undergo Coulomb interactions that can be generally classified in collisional and radiative losses [4]. These interactions include: [3]:

1. Bremsstrahlung radiation (radiative loss)
2. Soft collision (collisional loss)
3. Hard collision (collisional loss)

α-particles are charged particles that undergo collisional losses which are useful in radiation therapy. However, the advantages of α-particles will be addressed in the following sections.

Interactions of Photons with Matter

Photons are classified depending on their mode of production [3]; however, the most relevant type for this work are *gamma-rays*, which will be addressed in the following sections. Furthermore, depending on their energy, photons undergo a series of interactions, from which the *photoelectric effect, Compton scattering*, and *pair production* are the most predominant interactions in diagnostic and radiotherapy energy range [4]. Figure 2.1 shows the probability of interaction as a function of the incident photon energy and the atomic number of the absorber.

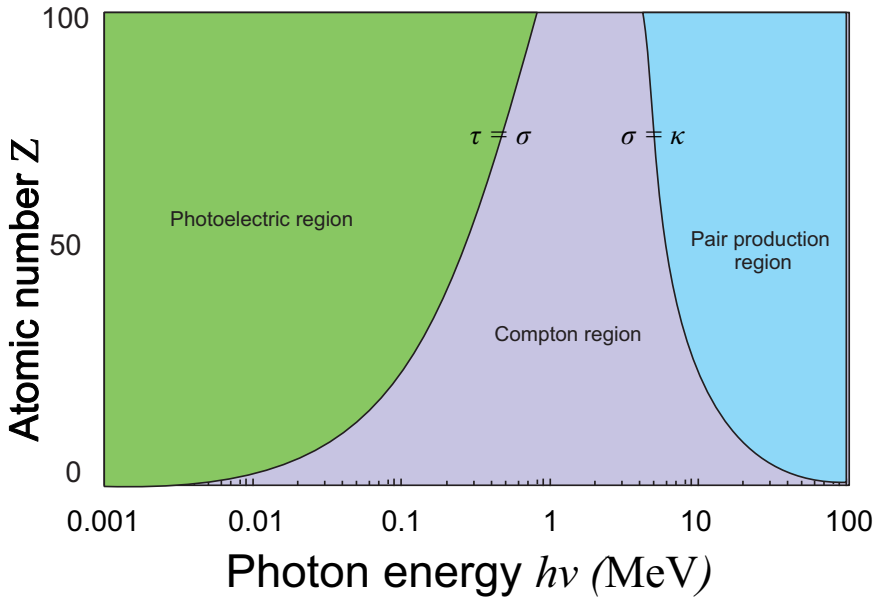

Figure 2.1: Plot of the probabilities of interactions for photons as a function of their energy. This plot was adapted from Podgorsak (2016). [3]

2.1.2 Linear Energy Transfer (LET) and RBE

Linear Energy Transfer (LET) is defined as the measurement of the rate of energy absorbed locally in the medium in a vicinity along the particle track per unit length [keV/μm] [2]. From now on, the medium or absorber will be referred to as tissue. Depending on the type of radiation, LET can be classified as **low LET** or **high LET** [2, 3]

Type	**Characteristics**	**Examples**	**Values [keV/μm]**
Low	Energy deposition in a relatively long range, more penetrating. For energies below 10 keV/μm	x-rays (250 kVp) γ-rays (Co-60) x-rays (3 MeV) Electrons (10 keV) Electrons (1 MeV)	2 0.3 0.3 2.3 0.25
High	Energy deposition in a relatively short range, less penetrating $\therefore$ more damaging for cells. For energies above 10 keV/μm	Neutrons (14 MeV) Protons (2 MeV) Carbon ions (100 MeV) Heavy ions (*e.g* α-particles)	12 17 160 100-2000

Table 2.2: Characteristics of low and high LET with some examples and their respective reported values. These LET values were taken from [3].

The LET of a particle in tissue has important implications for biological effects. All types of ionizing radiation have an associated LET and can produce the same biological effect, depending on the administered dose. However, the magnitude of the effect per unit dose is different for each type of ionizing radiation. In order to assess the effectiveness of each type of ionizing radiation, a comparison is made between the required dose of test radiation to produce the same biological effect produced by a dose of reference radiation. The relationship between the effectiveness of the test and reference radiation (dose of 250-kV x-rays) is given by the ***relative biological effectiveness (RBE)*** [2, 5]. RBE is defined as:

$$RBE = \frac{\text{Dose of 250-kV x-rays required to produce effect X}}{\text{Dose of test radiation required to produce effect X}}$$

Figure 2.2 shows the relationship between LET and RBE. It can be seen that initially with increasing LET, RBE increases as well. This is because high-LET ionizing radiation is more effective at producing cellular damage and most importantly, DNA damage. This DNA damage may result in a single-strand break (SSB) or double-strand break (DSB). DSBs are more deadly as they are more difficult for a cell to repair, and more likely to occur with high-LET radiation (for instance, α-particles). Furthermore, figure 2.2 exhibits a peak at 100 keV/μm in tissue, at which the probability of ionization events happening one after the other matches the width of the DNA double-helix, and hence the probability of an efficient DSB increase. Beyond this peak, RBE decreases due to the overkill effect, which means that the energy deposition exceeds the required amount to produce DSBs [2]. This efficiency is higher for α-particles given that these heavy particles (with a net positive charge), undergo collisional losses to transfer their energy. This energy-loss process is considered to be continuous throughout the distance traveled in the tissue, or range [4]. Compared to α-particles, electrons make a tortuous path through tissues, undergoing many collisions that change their direction multiple times. This is due to the much smaller mass of electrons compared to the large mass of α-particles [2]. Table 2.2 shows that α-particles have a LET from 100 keV/μm, therefore, the efficiency of producing DSBs is higher for α-particles.

Taking all these into consideration, it can be concluded that α-particles have a high

efficiency in killing cells. This characteristic can therefore be used in radiation therapy for cancer treatment.

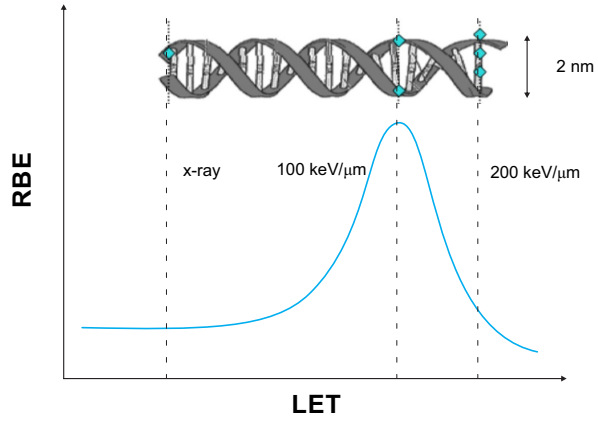

Figure 2.2: Plot of RBE as a function of LET showing DNA damage for different LET values. This figure was adapted from Kildea J. notes [5].

2.2 Radiation Therapy

Radiation therapy or *radiotherapy* is defined as the use of high-energy ionizing radiation (x-rays, γ-rays, electrons, or protons) to destroy or damage cancer cells. The aim of radiotherapy is to damage the DNA of cancer cells to trigger cell death. This high-energy ionizing radiation can be delivered by two means: by an external source or by internal sources placed inside the patient; the latter is also known as Brachytherapy [6].

2.2.1 External Beam Radiotherapy

In external beam radiotherapy conventionally used in the clinic, high-energy radiation is delivered to the tumor by radiation generators that produce high-energy photons or electrons. Photons penetrate deep into the tissue but also deposit their energy in the surrounding healthy tissue throughout their path. On the other hand, electron beams are used for superficial tumors or skin treatment due to their short range. Both types of beams are generated through a Linear Accelerator (LINAC).

2.2.2 Brachytherapy

In brachytherapy, radiation is usually administered from photon-emitting radiation sources (seeds) placed directly into or near the tumor, delivering high doses of ionizing radiation in a relatively small area. In contrast to external beam radiotherapy, brachytherapy allows a more localized dose distribution inside the tumor, therefore, sparing the healthy tissue. These seeds can be temporary or permanent depending on the type of cancer, its location inside the body, the general health of the patient, and additional treatments [6]. In addition to these sources, β-emitting (^{106}Ru [7], ^{90}Sr/^{90}Y [8,9]) are also used. Table 4.1 entitles the most used brachytherapy sources with their respective mode(s) of radioactive decay and their half-life.

Radionuclide	**Decay mode**	**Half-life**
^{131}Cs	Electron Capture (ϵ)	9.7 days
^{137}Cs	β^- and γ-rays	30.17 years
^{60}Co	β^- and γ-rays	5.26 years
^{90}Sr	β^-	28.79 years
^{90}Y	β^- and γ-rays	2.7 days
^{192}Ir	γ-rays	73.8 days
^{125}I	Electron Capture (ϵ)	59.6 days
^{103}Pd	Electron Capture (ϵ)	17.0 days
^{106}Ru	β^-	1.02 years
^{226}Ra	α	1599 years

Table 2.3: List of the radionuclides most used in brachytherapy with their respective modes of decay and their half-lives. This table was adapted from [10]

2.2.3 Radioactive Decay

Radioactive decay or *radioactivity* is defined as a spontaneous process in which an unstable nucleus (mother) transforms into a more stable nucleus (daughter). During this transformation process, energy is released from the mother in the form of ionizing radiation: α-particles, γ-rays, β^-, β^+, etc. [3,4]. The mode of radioactive decay depends on the type of nuclei involved but the ones of special interest for this project are α, β, and γ decay.

Alpha decay (α)

This mode of decay is more common in heavy elements (Z > 82 [3]) where an α-particle is emitted from the nucleus. α-particles are emitted with kinetic energy between 4-8 MeV with discrete values. The decay equation (equation 2.1) is shown below, where the atomic number Z decreases by 2 units, and the atomic mass number A decreases by 4, due to the fact that α-particles are made of 2 protons and 2 neutrons ($^4_2$He).

$$^A_Z X \rightarrow ^{A-4}_{Z-2} Y +^4_2 \alpha \tag{2.1}$$

Beta decay (β)

The β decay is classified into two different types of decay: β^- and β^+ from which, β^- is in the scope of this work. During this process, a neutron of the nucleus is transformed into a proton and an electron, therefore, the resulting daughter increases its atomic number Z by one unit. The atomic mass number A remains the same (isobaric decay). In a β^- decay energy spectrum, the maximum possible energy β^- particles can be released is given by the energy released during the transformation, known as the Q value. The average energy of the energy spectrum is given by one-third of the maximum energy ($< E >= \frac{E_{max}}{3}$).

$$n \rightarrow p^+ + e^- \overline{\nu} \tag{2.2}$$

$$^A_Z X \rightarrow ^A_{Z+1} Y + \beta^- + \overline{\nu} \tag{2.3}$$

Gamma decay (γ)

This process is the spontaneous emission of γ-photons from a nucleus in a metastable or excited state to a stable state. Equation 2.4 shows the decay for this mode of decay in which it can be seen that Z and A do not change, thus, this decay consists only in the emission of the excess energy. Since it deals with the transition from excited states to stable states, the energies of the emitted γ photon have discrete values.

$$ {}^{A}_{Z}X^{*} \rightarrow {}^{A}_{Z}X + \gamma \tag{2.4} $$

To describe the frequency of radioactive decay in a source, the term *activity* is used. *Activity* (A) is defined as the number of decays per unit time with SI units defined as the becquerel, Bq [s^{-1}]. Activity is described in equation 2.5. The old, but still used, the unit is the curie, Ci, which is equivalent to 3.7×10^{10} Bq [3, 4].

As the radioactive source decays into stable atoms, the activity decreases as a function of time. This behavior is described by the following equation:

$$ A(t) = A_0 e^{-\lambda t}, \tag{2.5} $$

where λ is known as the *decay constant* defined as:

$$ \lambda = \frac{ln(2)}{t_{1/2}} \tag{2.6} $$

Thus,

$$ A(t) = A_0 e^{-\frac{ln(2)}{t_{1/2}} t}. \tag{2.7} $$

Here $t_{1/2}$ is the *half-life* of the radionuclide, defined as the time at which the initial activity of a radioactive sample has decayed to 50% of its initial value.

2.2.4 Effects of α-particles in tissue

In previous sections, it was discussed that α-particles have a high efficiency in damaging cells' DNA by means of DSBs. The radiosensitivity of cells with low-LET radiation is related to the presence of oxygen – the more oxygen present in the cells, the more radiosensitive they will be. This is known as the oxygen effect [11,12]. The DNA chain can be damaged directly or indirectly by ionizing radiation. Direct DNA damage is produced when ionizing radiation directly interacts with the DNA depositing its energy. On the other hand, indirect DNA damage rises from the oxygen species, produced by ionizing radiation, reacting with the molecule [13,14]. When using indirect ionizing radiation (low-LET), the secondary electrons (electrons released from the medium) and the reactive oxygen species are responsible for

damaging the DNA molecule. Regarding oxygen levels, there can be hypoxic (low oxygen levels 1-5% O_2), normoxic (10-21% O_2), and hyperpoxia (> 21% O_2) conditions [15]. In cancer treatment, a solid tumor with hypoxic regions (hypoxic cells) is more radioresistant and will experience a lower level of DNA damage, resulting in a poorer treatment outcome. A way to overcome this is by using high-LET ionizing radiation, such as α-particles, given that they can cause direct DNA damage regardless of the oxygen levels and the cell cycle stage [11, 14]. In fact, to inactivate the cells' proliferative capability, just a few α-particles hits to the cell nucleus are necessary [11]. Therefore, α-particles have a great potential for radiotherapy. However, α-particles' range in tissue ($\sim$40–90 μm) [16, 17] is a significant limitation. This can be advantageous given that dose will be more localized or conformal inside the tumor. Since tumors are usually bigger than 100 μm, α-particles become ineffective to treat the entire volume. In order to overcome this limitation, several techniques have been introduced, such as Systemic ***alpha-radioimmunotherapy (α-RIT)*** and ***Diffusing Alpha-emitters Radiation Therapy (DaRT)***.

2.2.5 Diffusing Alpha-emitters Radiation Therapy (DaRT) in Brachytherapy

α-RIT: RIT involves the selective targeting of radionuclides to cancer-associated cell surface antigens using monoclonal antibodies [18]. Recently, α-RIT has demonstrated good effectiveness due to α-particles radiobiological properties and is preferred to treat small-size diseases like small cell clusters and micrometastases [19]. Zacherl, MJ. *et al.* (2021) [20] have reported clinical results using this technique.

DaRT: DaRT, on the other hand, is a novel brachytherapy technique with promising results for both pre-clinical and clinical trials, showing that it is an effective, potential, and safe treatment option for solid tumors [21–27].

DaRT consists of metal seeds with ^{224}Ra atoms ($t_{1/2}$ = 3.66 days) fixed to their surface, emitting a high-energy α-particle during its decay. Two main radioactive daughters are emitted and transported within the tumor by either diffusion or convection emitting more high-energy α-particles. Thanks to this transport, the contribution of α-particles to the dose

can reach a distance greater than 90 μm and extend to a range of several mm.

2.2.6 Seed Preparation and ^{224}Ra Decay Chain

The decay chain of ^{224}Ra is shown in figure 4.1. The chain starts with ^{228}Th ($t_{1/2}$ = 1.91 years), which allows it to be used as the generator of ^{224}Ra atoms [16]. Arazi *et al*(2007) [16], describes how the ^{224}Ra atoms are fixed to the surface of the seed according to the following procedure. The collection of ^{224}Ra is done using two main parts: a surface covered with a thin layer of ^{228}Th (^{228}Th generator) and a conducting stainless steel wire (⌀ 0.3 mm) placed at 5-15 mm away from the generator. Both components are electrically isolated inside an air-filled enclosure. The wire is held at a negative potential of 2-3 kV, therefore, all the electrostatic lines will converge at its tip. When ^{224}Ra is released ($\sim$ 100 KeV) by recoil from the generator, they thermalize the air molecules through collisions and are directed to the wire by means of the electric field lines. This resulted in collection efficiency of $\sim$95%. After this collection, the wire was heated at 450°C in a N_2 atmosphere, then characterized through α spectroscopy, immersed in water several times, and re-measured until the radium loss to water was about 1-2%. The final step was cutting the wire into small pieces of specific lengths: seeds. Each seed's activity ranged between 10 to 130 kBq.

Once ^{224}Ra is fixed to the surface of the seed, it α-decays into ^{220}Rn releasing a high-energy α-particle. ^{220}Rn is emitted by recoil from the seed and diffuses among the cells according to equation 2.8 defined by Arazi *et al* (2020) [28]:

$$\frac{\partial n_{Rn}}{\partial t} = D_{Rn}\nabla^2 n_{Rn} + s_{Rn} - \lambda_{Rn} n_{Rn}, \tag{2.8}$$

where D_{Rn} is the effective diffusion coefficient of ^{220}Rn in tissue, n_{Rn} is the local concentration of ^{220}Rn atoms, s_{Rn} is the ^{220}Rn source term (representing the recoil contribution from the source), and the λ_{Rn} is the decay constant of ^{224}Ra. The asymptotic solution to this equation (Eq. 2.10) leads to the following parameter known as the *effective diffusion length* of ^{220}Rn defined as:

$$L_{Rn} = \sqrt{\frac{D_{Rn}}{\lambda_{Rn} - \lambda_{Ra}}}. \tag{2.9}$$

$$n_{Rn}^{asy}(r,t) = \frac{P_{des}(Rn)\Gamma_{Ra}^{src}(0)e^{-\lambda_{Ra}t}}{4\pi D_{Rn}}\frac{e^{-r/L_{Rn}}}{r}, \tag{2.10}$$

where $P_{des}(Rn)$ is defined as the desorption probability of ^{220}Rn, and $\Gamma_{Ra}^{src}(0)$ is the initial activity of the source. In this study, two reference values for the effective diffusion coefficient are provided: $D_{Rn} : 1.9 \times 10^{-5} cm^2 s^{-1}$, and $D_{Rn} : 0.5 \times 10^{-5} cm^2 s^{-1}$ which yield two diffusion lengths of 0.39 mm and 0.20 mm, respectively.

^{220}Rn α-decays into ^{216}Po, another α-emitter radionuclide. However, due to its short half-life, it is assumed that it decays in the same place where it was generated. It is ^{212}Pb that contributes to further extending the distance at which α-particles deposit their energy. This radionuclide is transported through the bloodstream by means of lead-binding proteins. The diffusion of ^{212}Pb is governed by a similar diffusion equation:

$$\frac{\partial n_{Pb}}{\partial t} = D_{Pb}\nabla^2 n_{Pb} + s_{Pb} - \lambda_{Pb} n_{Pb} - \alpha_{Pb} n_{Pb} \tag{2.11}$$

The asymptotic solution to this equation (equation 2.13) also leads to the following diffusion length for ^{212}Pb:

$$L_{Pb} = \sqrt{\frac{D_{Pb}}{\lambda_{Pb} + \alpha_{Pb} - \lambda_{Ra}}} \tag{2.12}$$

$$n_{Pb}^{asy}(r,t) = \left(A_{Pb}\frac{e^{-r/L_{Rn}}}{r} + B_{Pb}\frac{e^{-r/L_{Pb}}}{r} \right) e^{-\lambda_{Ra}t}, \tag{2.13}$$

Where D_{Pb} is the *effective diffusion coefficient* of ^{212}Pb in tissue, α_{Pb} is the leakage rate coefficient, λ_{Pb} and λ_{Ra} are the decay constants of ^{212}Pb and ^{224}Ra, respectively, and A_{Pb} and B_{Pb} are coefficients defined in equations 2.14 and 2.15. For this diffusion length, this study reports an experimental diffusion length value of approximately 0.8 mm obtained from tumor histologies [28]. Arazi's study reports that these diffusion lengths determine the spatial distribution of the diffusing atoms, and therefore, give an idea of the distance at which α-particles can deposit their energy.

$$A_{Pb} = \left(\frac{L_{Rn}^2 L_{Pb}^2}{L_{Rn}^2 - L_{Pb}^2} \right) \frac{\lambda_{Rn}}{D_{Pb}} \frac{P_{des}(Rn)\Gamma_{Ra}^{src}(0)}{4\pi D_{Rn}} \tag{2.14}$$

$$B_{Pb} = \frac{\left(P_{des}^{eff}(Pb) - P_{des}(Rn)\right)\Gamma_{Ra}^{src}(0)}{4\pi D_{Pb}} - A_{Pb}, \tag{2.15}$$

where $P_{des}^{eff}(Pb)$ is the effective desorption probability. ^{212}Pb β-decays into ^{212}Bi which can either α- or β-decay into ^{208}Tl or ^{212}Po, respectively. These daughters decay into the stable lead (^{208}Pb). From figure 2.3, it can be seen that regardless of the decay mode that the daughter ^{212}Bi undergoes, one simple decay of ^{224}Ra contributes with four high-energy α-particles. Furthermore, throughout the entire decay chain, some daughters may decay into metastable/excited states resulting in the emission of γ-photons.

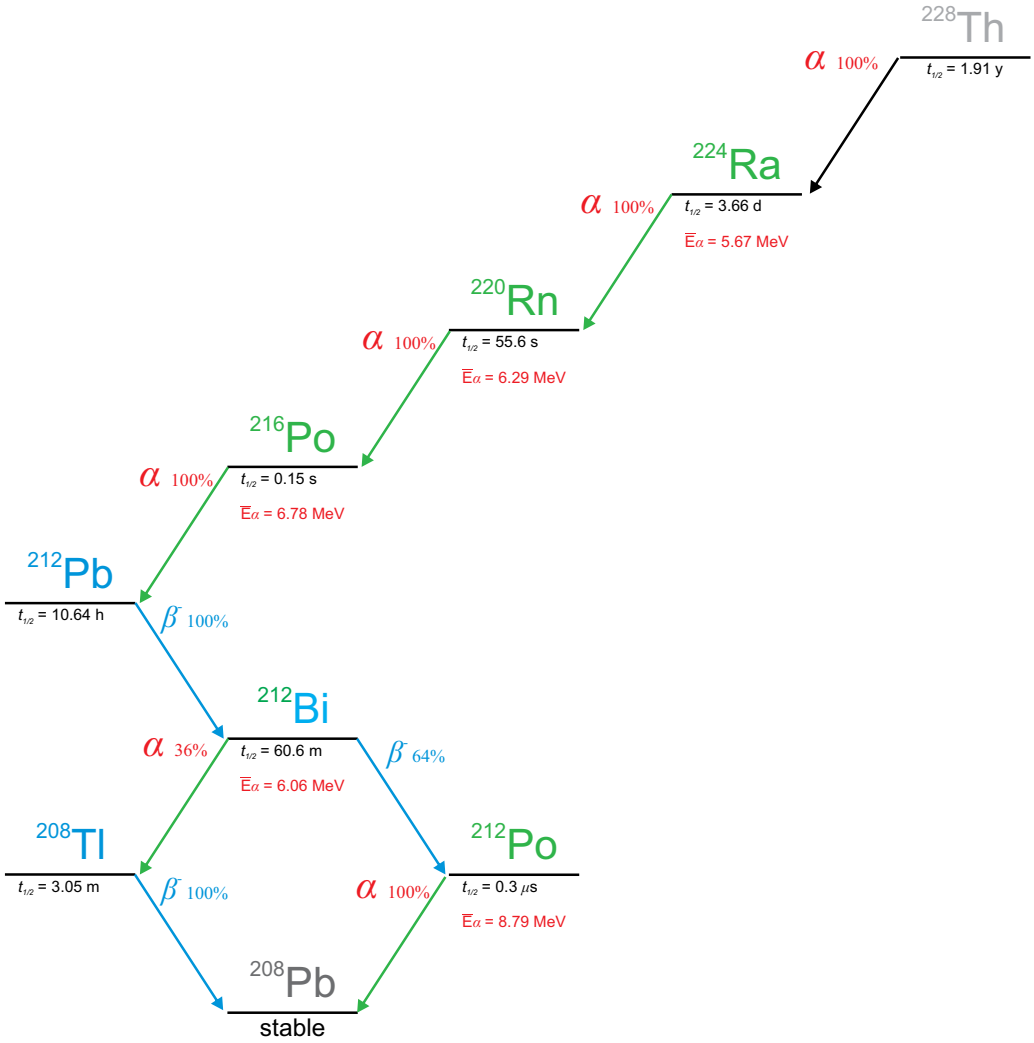

Figure 2.3: Scheme of the decay chain of ^{224}Ra showing each α-decaying (green) and β-decaying (blue) daughter emissions and their respective energies and probabilities.

The short half-life of ^{224}Ra, allows quick clinical outcomes [21] and corresponding

dosimetric measurements.

2.3 Dosimetry and Radiation Detection

All types of ionizing radiation transfer energy to the medium by means of directly and indirectly ionizing radiation resulting in a quantity known as ***absorbed dose (D)*** [Gy]. The *absorbed dose* is formally defined as *the expectation value of the energy imparted to matter per unit mass at a point* [29]. Another concept that derives from the absorbed dose and that will be used in this project is ***dose rate*** ($\dot{D}$) which is formally defined as the *absorbed dose per unit time* given in [Gy/hr] [29].

The majority of the sources used in brachytherapy are photon-emitting sources, therefore, a dosimetry protocol for these sources has already been developed.

2.3.1 TG-43

The American Association of Physicists in Medicine (AAPM) Task Group No. 43 published a protocol for brachytherapy dose calculation: TG-43. This protocol was originally published in 1995 and has been updated with significant improvements for dose calculations in brachytherapy dosimetry [30]. TG-43 provides dose calculation formalism for 2D cylindrical symmetric line sources and 1D point sources.

This formalism applies to sources with cylindrically symmetric dose distributions with respect to the source's longitudinal axis. As this dose calculation applies to photon-emitting sources, a similar formalism for α-dosimetry is required due to the recent increase in the use of α-particles in radiotherapy [31–35].

2.3.2 Alpha Particle Dosimetry using Radiochromic Films

Radiation detectors operate under the principle of interaction of ionizing radiation with matter and are used to characterize and quantify radiation from a given source. There are different types of detectors, but *radiochromic film* detectors are of special interest in this project due to their advantages; for example, they are used as dosimeters for low- to high-

dose ranges (0.1-1000 Gy); they are stable and have a high spatial resolution; they are easy to handle [36], and do not require any chemical process for data analysis. Radiochromic films are chemical detectors made of a monomeric (or mix of monomers) emulsion, also known as the active layer, placed over a flexible polyester film base. These detectors operate under the principle of radiochromic reactions, which are initiated when visible, ultraviolet, or ionizing radiation polymerizes the monomers in a process known as photo-polymerization. As a result of this photo-polymerization, the film darkens in the exposed area. A dosimetric signal can be obtained from this darkening given that it is proportional to the absorbed dose in the active layer of the film. However, each radiochromic film has its own absorption spectrum which has to be measured for film analysis. Radiochromic films must be calibrated before performing any dose measurements by means of obtaining the Hurter and Driffield (H&D) curve, which should include the dose region of interest to be measured. Figure 2.4 shows an example of a H&D curve for the External Beam Therapy (EBT2) film. This plot of net optical density (netOD) as a function of the absorbed dose is used as the calibration curve for a specific film batch and allows the determination of the dose delivered to a radiochromic film from measured netOD values [3].

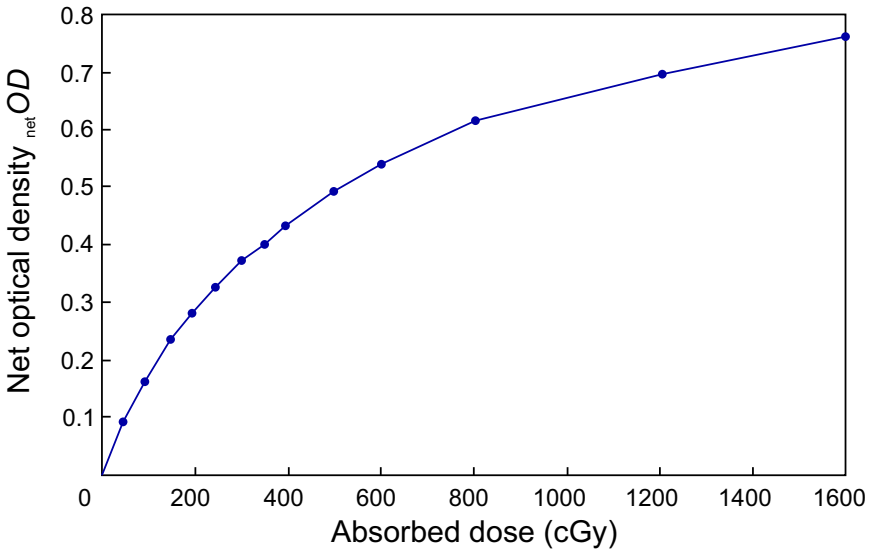

Figure 2.4: Example of the H&D sensitometric curve of the EBT2 for dose calibration. Figure adapted from Podgorsak E.B. (2016) [3].

Radiochromic films are a good option to be used for quantitative photon beam dosimetry and photon-based film dosimetry protocols have been completed in detail [37–40]. There are

a few works that have adapted photon-film dosimetry to α-particles using the GafChromic® External Beam Therapy (EBT3) film [41–43].

The EBT3 film is a three-layer film made of an active layer placed between two matte polyester base substrates (see figure 2.5). These protective substrates completely prevent α-particles from reaching the active layer and producing a response in the film. The previous work reported the use of a peeling-off method to study the response of this film to α radiation using a ^{241}Am source and performed an analysis of the net optical density to determine the absorbed dose due to alpha particles.

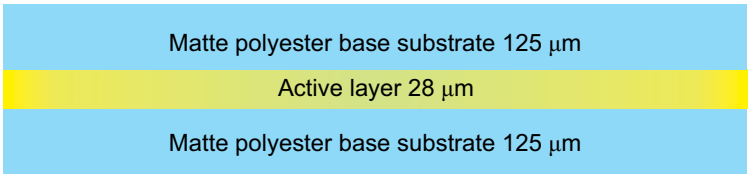

Figure 2.5: Scheme of the EBT3 film showing its thickness and order of the components.

However, the authors only report experimental results; no Monte Carlo (MC) simulations were performed in these studies. There are even fewer published studies concerning MC simulations [44, 45] for the GafChromic® EBT3 film.

As for DaRT dosimetry, this technique emits α-particles which range in tissue is of the order of few μm. Therefore, an α-based dosimetry detector is challenging and is needed for clinical practice purposes.

Given the fact that α-based therapy is a promising field, any type of experimental results should be benchmarked with MC simulations. MC simulations in Medical Physics provide useful information for any experimental setup since they allow to model of complex geometries and track each type of radiation produced for well-established physics libraries.

2.4 Monte Carlo Method

MC simulations have applications in dosimetry given that the electromagnetic processes, dimensions, materials, and composition of a radioactive source and detector can be accurately described to calculate the absorbed dose or any other quantity of interest. Furthermore, the tracking of each particle generated during the simulation allows the scoring of energy

deposition in the absorber. The simulated sources can go from a simple small radioactive source to complex geometries like a LINAC. As for detectors, these also include simple and complex geometries. An example of a simple-geometry detector could be the unlaminated GafChromic® EBT3 film. When performing simulations in Medical Physics or in any other research field, these simulations are based on the MC method.

2.4.1 Geant4 Simulation Toolkit

Geant4 is a simulation toolkit written in C++ programming language developed by the European Organization for Nuclear Research (CERN) designed to simulate the interactions of radiation through matter by sampling from different probability distributions [46,47]. Such sampling is done on the total interaction cross-section, the magnitude of such interactions, and the angular differential cross-sections. The sampling of these cross sections will allow determining the step length of the particle to transport it to a different position, the type of interaction, and the energy and direction of the generated particles, respectively. The Geant4 simulation toolkit allows the user to define and model complex geometries with different materials, define and generate radiation sources (external beams or radionuclides) with energies from few eV up to high-energies such as PeV, and score quantities of interest (energy deposited, absorbed dose, kerma). Geant4 generates primary particles that will produce secondary particles through the sampled electromagnetic processes, both types of particles will have different interactions in the medium that can be tracked and scored. To score quantities of interest, arrays of small scoring volumes can be defined to serve as sensitive radiation detectors [46, 48]. Therefore, MC-based user codes are a powerful tool that can be used to calibrate films for α-dosimetry and develop and assess new detector technology for DaRT.

Chapter 3

Body of Thesis

Investigation of dosimetric characteristics of EBT3 model GafChromic® film for alpha particle radiation

Victor D. Diaz-Martinez[1†], Mélodie Cyr[1†], Slobodan Devic[1,3], Nada Tomic[1,3], David F. Lewis[4], Shirin A. Enger[1,2,3]

[1]Medical Physics Unit, Department of Oncology, Faculty of Medicine, McGill University, Montréal, Québec, Canada. [2]Research Institute of McGill University Health Centre, Montréal, Québec, Canada. [3]Lady Davis Institute for Medical Research, Jewish General Hospital, Montréal, Québec, Canada. [4]RC Film Consulting, 54 Benedict Rd. Monroe, CT, USA.

Victor D. Martinez: victor.diazmartinez@mail.mcgill.ca

Mélodie Cyr: melodie.cyr@mail.mcgill.ca

† Both authors contributed equally to this work.

Abstract

Background: In radiotherapy, it is essential to deliver prescribed doses to tumors while minimizing damage to surrounding healthy tissue. Accurate measurements of the absorbed

dose are required for this purpose. Gafchromic® external beam therapy (EBT) radiochromic films have been widely used in radiotherapy. While the dosimetric characteristics of the EBT3 model film have been extensively studied for photon and charged particle beams, few research has been completed on adapting photon-film dosimetry to α-particles. α-emitting radionuclides have gained popularity in cancer treatment due to their high linear energy transfer, short range in tissue, and ability to spare surrounding organs at risk, thereby achieving a more localized dose distribution to the tumor. Therefore, a dose-calibration film protocol for α-particles is required.

Purpose: The aim of this study was to develop a dose-calibration protocol for α-particles using Monte Carlo (MC) simulations and measurements with unlaminated EBT3 films.

Methods: In this study, a MC-based software was developed using the Geant4 simulation toolkit to model and simulate an ^{241}Am source and an unlaminated EBT3 film. Two simulations were performed: one with voxelized geometries of the EBT3 active volume composition and the other using water. The dose rate was calculated within a region of interest in the voxelized geometries. Additionally, unlaminated EBT3 film pieces were irradiated with the ^{241}Am source at various exposure times inside a black box. For comparison, film irradiations were also performed using a 6 MV photon beam from a Varian TrueBeam machine. The simulated dose rate was used to convert the exposure times into absorbed doses. The irradiated films were scanned, and an in-house Python script was used to analyze the normalized pixel values for the green channel.

Results: The ^{241}Am photon and α-particle energy spectra obtained from the simulations were in good agreement with reported databases, with differences ranging from 0.036% to 0.516% and from 0.001% to 0.006% respectively. Due to the short range of α-particles, there was no energy deposition in the voxels outside the active ^{241}Am source region projected onto the film surface. Thus, the total dose rate within the voxels covering the source was 1.096 $\pm$ 0.008 Gy/min for LiPCDA and 1.113 $\pm$ 0.006 Gy/min in water.

This indicates that the sensitive layer of the unlaminated EBT3 film is water equivalent for the beam quality emitted by ^{241}Am. The results were also in good agreement with published work. A novel approach was employed in α-film dosimetry by using an exponential fit for the green channel, which showed promising results by reducing the uncertainty in dose estimation within a 5% margin. Although the statistical analysis did not reveal any significant differences between the photon and α calibration curves, the dose-response curves exhibited the expected behavior.

Conclusions: The developed MC software accurately recreated the experimental setup for α-dosimetry using radiochromic film and obtained reliable results. Unlaminated EBT3 film is suitable for the dosimetry of α-radiation at low doses and can be used in conjunction with other unlaminated GafChromic® films for quality assurance and research purposes.

3.1 Introduction

Radiotherapy cancer treatments, such as advanced external beam radiotherapy, must maximize ionizing radiation to a tumor while minimizing the dose to healthy surrounding tissue. Treatment verification and quality assurance (QA) are often performed on the equipment delivering these advanced radiotherapy treatments, using dosimeters to ensure the delivery of an accurate dose to the tumor. One example of dosimeters commonly used is Gafchromic® films. The external beam therapy (EBT) model of Gafchromic® film has been used in most of the applications of radiation therapy in the last decades [49] and was specifically developed for the needs of EBT dosimetry. Gafchromic® radiochromic EBT films have many advantages, such as a high level of achievable accuracy for a wide range of dose values (0.1-1000 Gy), high spatial resolution, no chemical processing, small energy dependency, almost dose rate independency, and ease of handling [36, 37, 45, 50–52]. The EBT3 is a model of Gafchromic® film and has a near tissue equivalent active layer. The recommended dose range for EBT3 model Gafchromic® film is from 0.1 cGy up to 10 Gy, which covers many dosimetric applications in conventional hyper-fractionated

photon-based radiotherapy [53].

EBT film dosimetry protocols for photons have been reported in great detail [37–40] and dose-response characteristics of these films for charged particle beams such as an electron, proton, and carbon-ion beams have been reported by several groups [49, 52, 54]. Martisikova *et al.* (2008) [52] studied the effectiveness and total uncertainty in the net optical density (OD_{net}) of EBT GafChromic® films irradiated with a ^{60}Co source to assess the EBT films suitability for quantitative dosimetry in photon beams. The authors concluded that although EBT GafChromic® films have remarkable advantages, there are certain factors that need to be considered in order to achieve 5% accuracy in the dose delivered to a patient. Such factors are the statistical spread of the pixel values in a region of interest (ROI), film homogeneity, scan-to-scan stability, longtime stability of the scanner, light scattering, film development, and effect of the scanner light on the film [52].

Sorriaux *et al.* (2013) [49] evaluated the uncertainties and characteristics of the EBT3 films in photon, electron, and proton radiotherapy and concluded that the low combined uncertainty observed and the small dependency on radiation quality (beam-type and energy) make EBT3 a promising candidate for dosimetry in various applications. Castriconi *et al.* (2013) [54] investigated the dose-response of EBT3 films to proton and carbon-ion clinical beams in comparison with conventional photon radiotherapy beams. The authors found that for protons, the response of EBT3 film in the plateau of the depth-dose curve is not different from that of photons, within experimental uncertainties. For carbon-ions; however, an energy-dependent under-response of EBT3 film was observed. An under-response in the Bragg peak region was observed for both protons and carbon ions. EBT3 has shown energy dependencies for photon radiation to energies that are lower than 100 keV [53].

During the past few years, treatment of cancer with α-particle emitting radionuclides has gained popularity [31–35]. The energy of emitted α-particles from these radionuclides (^{211}At, ^{213}Bi, ^{223}Ra, ^{225}Ac) varies from 5 to 9 MeV with a range of 40–100 μm in water or soft tissue. These α-particles have a linear energy transfer (LET) range of 80–110 keV/μm, which is three times greater at the Bragg peak [55]. Furthermore, the short range of α-particles in tissue spares the surrounding organs at risk, achieving a more localized dose distribution. To further investigate the dosimetry of α-particles with radiochromic films, a dose-calibration

film protocol for α-particles is required.

To date, only a few published papers have adapted the photon-film dosimetry to α-particles. Mustaqim *et al.* (2018), Ng *et al.* (2016) and Mukherjee *et al.* (2015) [41–43] irradiated EBT3 films with an ^{241}Am source and studied the film response to α-radiation by peeling off one of the film protective layers. This peeling-off method was performed to ensure that α-particles were not stopped in the protective layer before reaching the active layer of the film. However, one limitation of the above-mentioned studies was that the peeling-off of the protective layer might have damaged the active layer and hence, affected the response [43]. Furthermore, only experimental results were reported along with theoretical α-particle dose calculations without benchmarking with the Monte Carlo (MC) method.

The aim of this study was to develop a dose-calibration protocol for α-particles, through MC simulations and film response measurements with unlaminated EBT3 model GafChromic® films.

3.2 Methods

3.2.1 Unlaminated EBT3 Model GafChromic® Film and Source Characteristics

Unlaminated EBT3 model GafChromic® films (Ln 06171901 and Ln 11181901P1) were specially ordered from Ashland [53] to be used in this study. Unlike the usual EBT3 model of the GafChromic® film, that consists of a 28 μm thick active layer sandwiched between two 125 μm thick polyester substrates for protection, the unlaminated EBT3 model GafChromic® film consist of an active lithium salt layer (lithium pentacosa-10, 12-diynoate (LiPCDA)) with 14 μm thickness placed on one protective layer of matte-polyester substrate with the thickness of 125 μm. Figure 3.1 shows a comparison between the laminated and unlaminated films: figures 3.1a and 3.1b, respectively. Figure 3.1b and table 3.1 present the composition of the unlaminated EBT3 model GafChromic® film used in this study.

(a) **(b)**

Figure 3.1: Order of the different layers for the a) laminated and b) unlaminated EBT3 model GafChromic® film including their respective thicknesses. Dimensions not to scale.

Layers	Thickness	Density	Composition [%]								
	[μm]	g/cm^3	H	Li	C	N	O	Na	Al	S	Cl
Active	14	1.15	8.65	0.63	50.01	0.64	32.37	0.35	6.57	0.24	0.54
Polyester	125	1.35	4.20	0.00	62.50	0.00	33.30	0.00	0.00	0.00	0.00

Table 3.1: Characteristics of the unlaminated EBT3 model GafChromic® film including the thickness, mass density, and elemental compositions.

An ^{241}Am type-A disk with a current activity of 30.02 kBq ($t_{1/2}$ = 432.2 y) purchased from Isotope Products Laboratories (California, USA) was used in this study. Figure 3.2 illustrates the source (3.2a) and details its components (3.2b). The source consists of an aluminum ring (outer ⌀ 25.4 mm, inner ⌀ 12.49 mm, 0.508 mm thick, density 2.699 g/cm^3) placed above a thin gold foil (⌀ 12.49 mm, 50 nm thick, density 100 $\mu g/cm^2$) covering the ^{241}Am source (⌀ 5 mm and 0.8 nm thick, density 13.67 g/cm^3). The gold cover is meant to protect the active ^{241}Am layer. The active layer is placed on a solid platinum foil (⌀ 15.87 mm, 0.127 mm thick, density 21.45 g/cm^3) which is placed on top of an aluminum plug (⌀ 24.13 mm, 1.93 mm thick, density 2.699 g/cm^3).

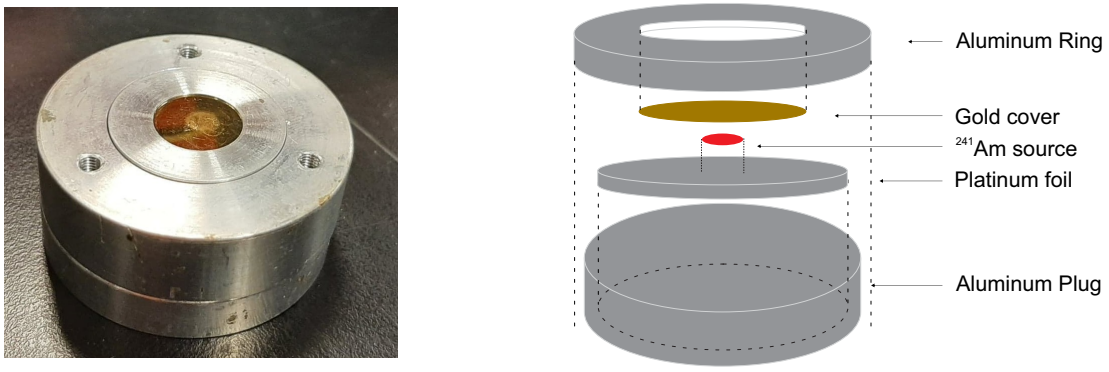

(a) **(b)**

Figure 3.2: a) The ^{241}Am type-A source b) detailed components of the source consisting of an aluminum ring placed on top of the gold cover, the active ^{241}Am source volume, platinum foil, and an aluminum plug.

3.2.2 Monte Carlo Simulations

An in-house MC-based user code built on the Geant4 (Version 10.7 Patch-02) simulation toolkit [46] and an in-house Matlab (version R2021a) script were developed to perform the simulations and dose rate calculations. The geometry, material composition, and characteristics of the ^{241}Am source and the unlaminated EBT3 model GafChromic® film were modeled in detail to accurately reproduce the experimental setup that will be described in the following section. The results of the MC simulations include the emitted energy spectra of the ^{241}Am source (α, γ, and characteristic x-rays energy spectrum) and the calculated dose rate. The α and γ energies were compared with the database from the IAEA [56], while the energies of the characteristic x-rays were compared with the NIST X-ray Transition Energy Database [57]. As for the simulations, the input parameters for the simulation and the calculated dose rate were compared to the published work of Ramos-Moreira (2020) [44] for validation.

The ^{241}Am source was modeled according to the specifications given in the previous section. ^{241}Am atoms were randomly sampled to decay isotropically from the active source volume. Next, a film with a surface area of 6.35×5.08 cm^2 and the identical geometry as depicted in figure 3.1 was placed on top of the source with the active layer facing the source. Energy depositions were scored in the active layer of the film, which was segmented into 600×600 voxels, each with a size of $0.105 \times 0.084 \times 0.014$ mm^3. Two sets of simulations were performed the first set with the material composition of the unlaminated film given in table 3.1 and the second set with water (density 1.0 g/cm^3) as scoring material. For both sets of simulations, 1×10^8 decay events were simulated to ensure type A statistical uncertainty of 0.001% in each voxel inside the ROI.

The source decay was handled through Geant4 radioactive decay physics with the explicit simulation of the nuclear decay, where the radioactive decay data was taken from the Evaluated Nuclear Structure Data File (ENSDF) (Brookhaven National Laboratory, National Nuclear Data Centre). This eliminates the need to include hard-coded decay energy spectra for the source. The interactions of the α-particles with the medium in the simulations were handled through the G4EmStandardPhysics_option3 package, used for proton and ion therapy [58, 59]. This Geant4 package uses the stopping powers from the

International Commission on Radiation Units and Measurements (ICRU) 49 report for energies < 8 MeV [60]. A production cutoff of 4.6 μm was defined for secondary particles. In accordance with the recommendations of the American Association of Physicists in Medicine Task Group 268 report [61], all the parameters used in the simulations are presented in table 4.2. The simulations were performed on the Cedar cluster of Digital Research Alliance of Canada [62].

Item	**Description**	**References**
Toolkit	Geant4 version 10.02 P2	Agostinelli *et al* [46]
Cross-sections	Penelope Stopping powers database (ICRU49)	Barol *et al* [63] Mendoza *et al* [60]
Validation	The ^{241}Am spectrum was compared to the reported values from the IAEA and NIST databases. The dose rate results were compared to published work	IAEA Live Chart of Nuclides [56], NIST X-ray Transition Energy Database [57] Ramos-Moreira, Lee K. *et al.* [44, 45]
Source description	^{241}Am type-A disk source	Isotope Products Laboratories (California, USA)
Production Cut-off for all particles	4.6 μm	
Statistical uncertainty	Batch statistics error estimation method	FLUKA [64], A. F. Bielajew [65]

Table 3.2: Summary of parameters used for Monte Carlo simulation

Dose rate per voxel calculations was performed with an in-house Matlab script by using the energy deposition map obtained from the MC simulations in each scoring voxel of the simulated unlaminated EBT3 model GafChromic® film. An ROI of 1 mm in diameter was taken to obtain the mean dose rate and its standard deviation. The dose rate value was normalized to the total number of particles simulated and the actual activity of the source. This last factor will have an impact on the final normalized dose rate. Equations 3.1 and 3.2 shows the dose rate normalization used for this study and the one used in the publication by Ramos-Moreira (2020), respectively.

$$\dot{D} = \frac{D_{sim} \times Act_{source}}{N_{emitted}} \left[\frac{Gy}{s}\right] \tag{3.1}$$

where D_{sim} is the simulated scored dose in the scoring voxels, Act_{source} is the activity of the source, and $N_{emitted}$ is the number of *emitted* particles (simulated histories).

$$\dot{D} = \frac{D_{sim} \times A_{target} \times \Phi}{N_{scored}} \left[\frac{Gy}{s}\right] \tag{3.2}$$

Where A_{target} is the area of the target, N_{scored} is the number of particles *scored* in the target, and Φ is given by:

$$\Phi = \frac{N_{scored} \times Act_{source}}{N_{emitted} \times A_{target}} \left[\frac{1}{cm^2 \cdot s}\right] \tag{3.3}$$

By substituting equation 3.3 into equation 3.2, equation 3.1 is obtained, showing that depending on the activity of the source that is being used, the dose rate will be different.

These dose rate results from the simulations in our study were used to convert the irradiation exposure times of the unlaminated EBT3 model GafChromic® film into dose in order to obtain dose-calibration curves.

Film Irradiation & Scanning

Film irradiations were performed using the unlaminated EBT3 model GafChromic® film and the ^{241}Am type-A disk source described in the previous section. The films were cut into 6.35 × 5.08 cm^2 pieces using a guillotine paper cutter. The films were cut longitudinally and a landscape scanning orientation was followed throughout the entirety of the study. The ^{241}Am source, was placed inside a metal box to isolate it from external UV light (mimicking a dark box environment). Films were placed on top of the ^{241}Am source with the active layer in contact with the gold cover as illustrated in figure 3.3. Exposure times varied for deposited dose in the range of 0 to 1184 Gy according to the dose rate calculated with the MC simulations. Table 3.3 in the Results section presents the film number, film exposure time in hours, and dose in Gy for reference.

Irradiated films were scanned using an Epson Expression 10000 XL scanner before and after irradiations, and the images were saved as a Tagged Image File Format (tiff). The films were scanned at 127 dpi in the 48-bit RGB mode (16 bits per color). All scanned images

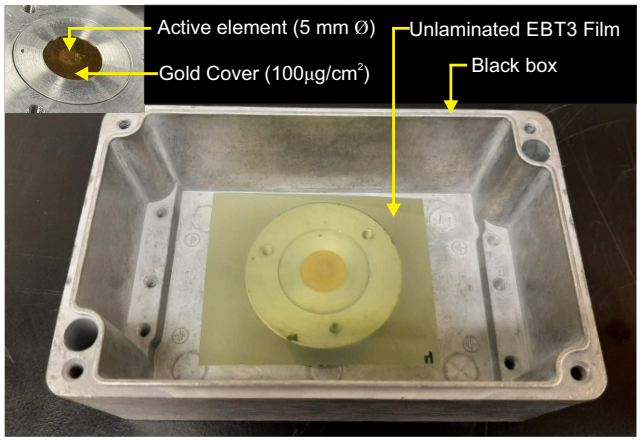

Figure 3.3: Experimental setup for film irradiation showing the ^{241}Am type-A disk source inside the metal box and the piece of the unlaminated EBT3 model GafChromic® film placed on top of the source

were analyzed using an in-house Python 3.8.3 script to acquire the pixel values (PV) for the green color channel. An ROI of 1 x 1 mm^2 (5 x 5 pixels) was taken for both film and MC simulations. The PV of the exposed region of the films was converted into *normalized pixel values* (PV_{norm}), which represents the film response at green color channel (Equation 3.4). The film irradiations were repeated three times to decrease the uncertainty. The calibration curve of the delivered dose of the PV_{norm} (equation 3.4) was fit with equation 3.5.

$$PV_{norm} = \left(\frac{PV_{background}}{PV_{irradiated}} - 1\right) \tag{3.4}$$

And the normalized data were fit with the:

$$y = ax + bx^n \tag{3.5}$$

With y being the dose in Gy, x the PV_{norm}, and a, b, n the fitting parameters of the polynomial correction to a linear form, and a was always forced to be zero. The data fitting and error analysis was taken from Devic *et al.* (2004) [66]. Consistent with prior publications, the plotted uncertainties were derived from the relative fit parameter uncertainties and experimental uncertainties added in quadrature [37–40].

A comparison was made between the α-particle and photon film dosimetry. To carry out this comparison, eight samples of the unlaminated EBT3 GafChromic® film (each measuring

2" x 4") were positioned at the center of a 10 x 10 cm^2 field size produced by a 6 MV TrueBeam accelerator (Varian Medical Systems, Palo Alto, CA). The films were placed at a source-to-surface distance of 100 cm and were covered with a 5 cm thick piece of solid water, while a 9 cm thick piece of solid water was positioned beneath the films to ensure appropriate scatter conditions. Each film was exposed to a different dose, ranging from 0 to 100 Gy, with increments of 2, 5, 10, 20, 50, 70, and 100 Gy. The ROI that was analyzed corresponded to a 2 x 2 mm^2 area at the center of each film.

The same scanner with the same scanning protocol used for the α film dosimetry was used. The PV_{norm} were calculated using the equation 3.4. The calibration curve i.e., the delivered dose of the PV_{norm} was fit with the same function used to fit the α film dosimetry data (equation 3.5).

3.3 Results

The results for both the MC simulation and the experimental irradiation are presented in the following subsections.

3.3.1 Monte Carlo Simulations

Through MC simulations, we determined that the two α-particle energies with the highest probability of being emitted from ^{241}Am decay were 5.44 and 5.48 MeV (see figure 3.4a). These values were in agreement with data previously reported by the IAEA [56], with a difference range of 0.001% to 0.006%. Figure 3.4b presents the simulated photon and characteristic x-ray spectrum from the ^{241}Am decay. It contains the two main photons emitted from the metastable states of ^{241}Am (26.31 and 59.54 keV) [67] and the characteristics L x-rays of the first daughter ^{237}Np (13.9, 17.81, 20.93, and 26.31 keV). These values were compared to the values reported by the NIST in their x-ray Transition Energy Database and the IAEA Live Chart of Nuclides data, [56, 57] and were found to be in good agreement with a range of difference between 0.036-0.516%. Furthermore, the shape of the photon/characteristic x-ray spectrum is similar to the ones reported by Demir D. *et al.* (2013) and Ramírez-Jiménez, F.J. (2006) [68, 69].

Figure 3.5a displays a map of the dose rate per voxel in a grid of 600×600 simulated voxels. The x and y values of each voxel correspond to the pixel size, and the dose rate values are depicted in the color scale corresponding to each pixel value. The scale in this figure highlights that the high-dose-rate values create a circular pattern in the central region of the film, corresponding to the shape of the active volume of the ^{241}Am source. Voxels with a dose rate of 0 Gy/min are illustrated in blue in figure 3.5a, as indicated by the color bar. This finding indicates that there was no energy deposition outside of the active ^{241}Am source volume, except for scattered radiation caused by the gold cover, which is represented by the differing dose-rate intensity halos present in this region. To investigate the uniformity of the high-dose-rate region, a 1 mm ⌀ ROI was selected in the most uniform section, as illustrated in figure 3.5b. The dose rate values for the LiPCDA active layer and water inside the ROI were found to be 1.096 ± 0.008 Gy/min and 1.113 ± 0.006 Gy/min, respectively, suggesting the water-like properties of LiPCDA. A profile was taken on figure 3.5a over the y-axis and normalized to the maximum dose rate value to illustrate the variation between the pixel dose rate values within the ROI, as shown in figure 3.5c. The calculated dose rate of 1.096 ± 0.008 Gy/min was compared with the one reported by Ramos-Moreira (2020) [44] whose dose rate was reported to be ∼2.4 Gy/min. The difference in dose rate is due to different simulation input parameters used in the two studies which are summarized in table 3.4.

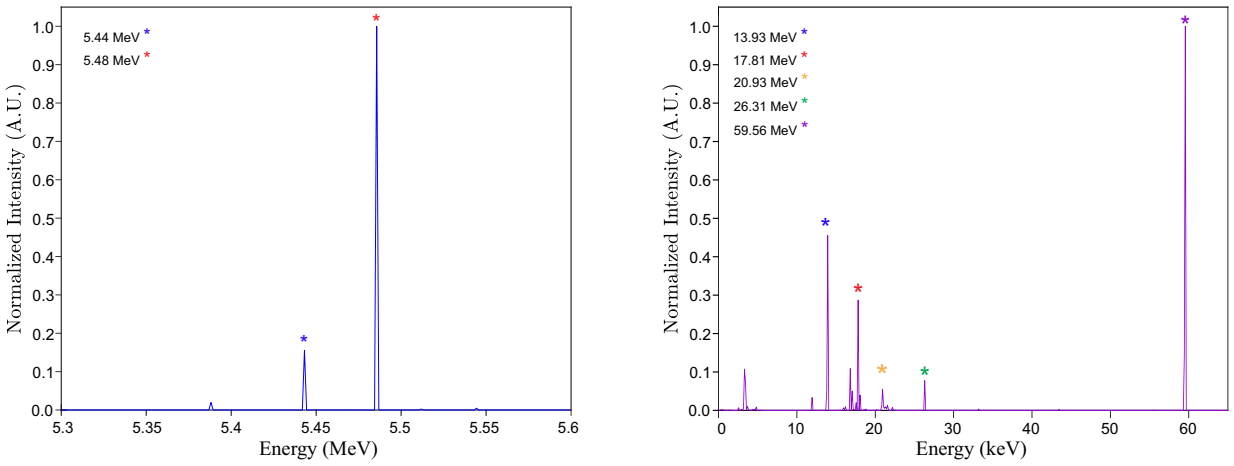

(a) (b)

Figure 3.4: a) α-particle with the two main relatively high-intensity energies and the b) photon spectrum of the ^{241}Am source containing the L-transition x-rays from ^{237}Np and the two main gamma photons emitted from ^{241}Am. The intensity of each plot was normalized to its maximum intensity value.

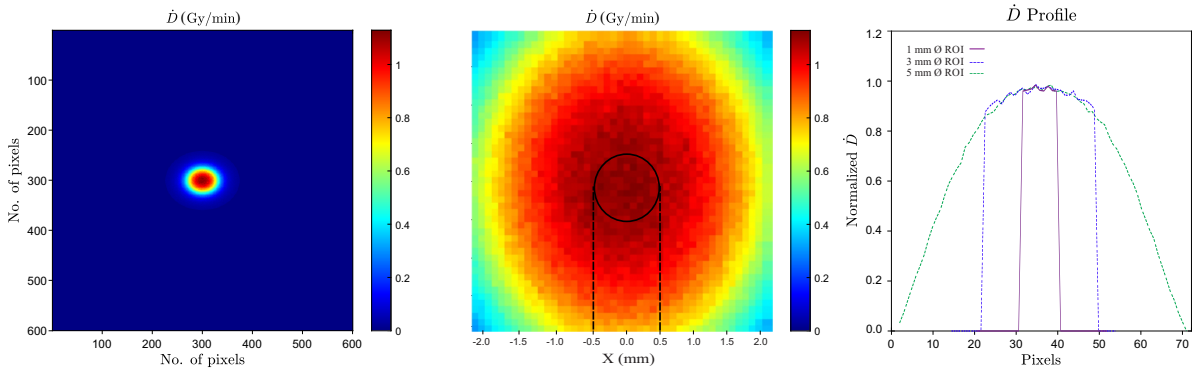

(a) (b) (c)

Figure 3.5: (a) Dose rate per voxel map obtained from the simulation, (b) the ROI of 1 mm in diameter over the most uniform part of the highlighted region of the dose rate per voxel map shown as the black circle. The light black dashed lines indicate the edges of the ROI located at -0.5 and 0.5 mm from the center of the ROI on both axes. (c) Represents profiles taken over the y-axis of the dose rate map only considering those values inside different ROI diameters: 5, 3, and 1 mm. These profiles illustrate the importance of the ROI size in the dose rate calculation due to the variation between each pixel. The 1 mm ∅ ROI is the one that allows a more uniform dose rate distribution.

3.3.2 Film Irradiations

The unlaminated EBT3 model GafChromic® film exhibited a clear response to the α-radiation, as seen in Figure 3.6. Similar to the results obtained from the MC simulations, a closer examination of the film response revealed a halo around the saturated region of the irradiation. Hence, the ROI for the irradiated film without the halo is a 1 x 1 mm^2 area,

which corresponds to the size of the saturated portion on the film from the active ^{241}Am source volume. The ROI was used in the calculation of the PV_{norm}.

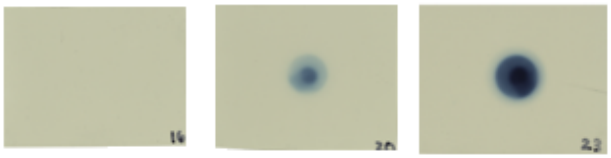

Figure 3.6: Response of the unlaminated EBT3 model GafChromic® film to ^{241}Am radiation. The absorbed doses were associated with films 0, 66 ± 0.02, and 1190 ± 0.23 Gy, from left to right.

Figure 3.7a illustrates the results of investigating the relationship between absorbed dose and PV_{norm} for film irradiation with both α-particles and a 6 MV photon beam. The green channel was exclusively used as it provides the most accurate representation for this film model [66]. Table 3.3 lists the film number, exposure time, PV_{norm} for the green channel, and absorbed dose in Gy for irradiation with the ^{241}Am source. However, for doses higher than 120 ± 0.044 Gy, the high film exposure and the scanner's limited sensitivity resulted in large error bars, making it difficult to obtain reliable results. Consequently, the higher doses of 710 ± 0.13 Gy and 1190 ± 0.23 Gy from the α-particle irradiation were eliminated to enhance the comparison of the results for the two radiation types, as shown in figure 3.7a. As seen in the figure, only the PV_{norm} is presented since its response function has a linear relationship in the dose ranges studied for MV photon beams [40].

As outlined in the methods section, the PV_{norm} data was fitted using equation 3.5. Based on this function, the dose error, experimental uncertainty, fit uncertainty, and total uncertainty were calculated for the α-irradiation from previously published data for photons [37–40]. The results are presented as a percentage of the absorbed dose and plotted in figure 3.7b as a function of dose. The experimental uncertainty, fit uncertainty, and total uncertainties are under 5%. However, the relative dose error has a large outlier at the dose 2.4 ± 0.01 Gy of 24%. Since this dose is small resulting in a small signal seen on the scanned image, the PV could not be properly sampled from the scanned image, resulting in a higher dose error. This is a limitation of the technique used.

Film Number	Time (hr)	PV_{norm}	Dose (Gy)
0	0	4.854×10^{-4}	0
1	0.0361	0.0233	2.37
2	0.1667	0.0849	11.0
3	0.3333	0.1433	22.0
4	1	0.2775	65.7
5	1.8	0.3861	118
6	10.8	0.7474	710
7	18	0.8519	1184

Table 3.3: The film number, the film exposure time, the PV_{norm}, and the absorbed dose in Gy for irradiation with the ^{241}Am source. The exposure time was converted into the absorbed dose using the dose rate of 1.096 $\pm$ 0.008 Gy/min, resulted from the MC simulations.

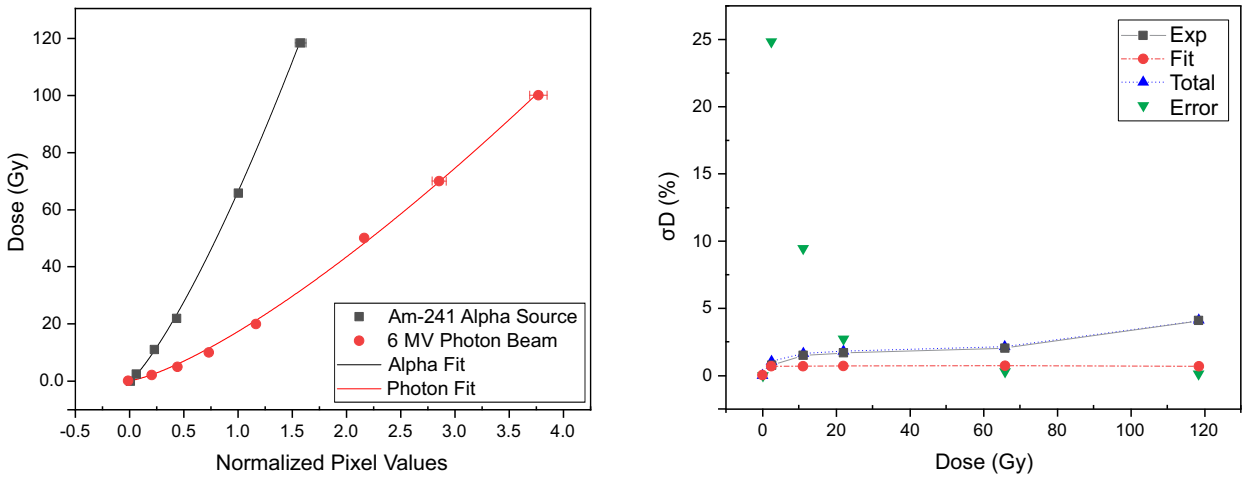

Figure 3.7: (a) Calibration curves of the PV_{norm} for α-irradiated and 6 MV photon irradiated films.The higher doses of 710 $\pm$ 0.13 Gy and 1190 $\pm$ 0.23 Gy have been removed for better comparison between the two radiation modalities. (b) Uncertainty and error analysis for the α-irradiation from the fit, experimental, total uncertainties, and relative dose error.

3.4 Discussion

Radiochromic films have proven useful in the dosimetry of various radiation qualities besides photons. Emerging treatment options, such as targeted internal therapy that utilizes α-particle emitters to treat micro-metastatic diseases [43] and a new brachytherapy treatment option for solid tumors using diffusing alpha-emitters released from ^{224}Ra-loaded seeds known as Diffusing alpha-emitters Radiation Therapy (DaRT) [16,26], are examples of applications

that can benefit from GafChromic® film measurements.

In this study, a dose-calibration protocol for α-particles, through MC simulations and measurements with unlaminated EBT3 model GafChromic® films, was developed. The irradiation of the unlaminated EBT3 model GafChromic® was performed with a 30.02 kBq ^{241}Am source and was compared to a 6 MV photon beam irradiation.

3.4.1 Monte Carlo Simulations

An MC-based user-code was developed to simulate the decay of an ^{241}Am source and calculate the dose rate for calibration of the unlaminated EBT3 model GafChromic® film irradiated with this α-particle emitter source. In order to validate the developed software, the main peak values of the decay energy spectra were compared to those values from the database published by the IAEA and NIST [56, 57]. The α-particles energies were compared with the IAEA database having a different range of 0.001% to 0.006%. The photon spectrum including the characteristic x-rays and γ-photons were compared to the NIST and the IAEA, respectively. The photon energy spectrum was found to be in good agreement since there was a 0.036-0.516% range difference. This indicates that the simulation of the active source is accurate. Furthermore, the shape of the energy spectrum is the same as the ones measured in published work by Demir *et al.* (2013) [68] and Ramirez-Jimenez, F. J. (2006) [69]. The dose rate was compared with results obtained by Ramos-Moreira (2020) [44], which also studied the response of EBT3 model GafChromic® films to α-radiation. In our study, the dose rate for the LiPCDA active layer was 1.096 ± 0.008 Gy/min, while the value reported by Ramos-Moreira (2020) was ~ 2.4 Gy/min. The difference between these dose rates is due to different simulation input parameters used in the two studies summarized in table 3.4.

The study conducted by Ramos-Moreira (2020) excluded the two emitted photons (26.31 and 59.56 keV) during the decay of ^{241}Am from the simulations due to limitations with TOPAS [70], which is a wrapper to the Geant4 Simulation Toolkit. In spite of that, in order to achieve a more accurate representation of the real source emissions, these photons and the L characteristic x-rays were included in our simulations as shown in figure 3.4b. However, according to previous research by Lee, K. H. *et al.* (2018) and Lee, K. M. *et al.* (2016) [45, 71], the contribution of these photons to the absorbed dose is minimal. In

addition, Ramos-Moreira (2020) utilized a version of TOPAS that lacked a definition of the material americium. As a workaround, the authors simulated an active source volume made of hafnium (Hf) instead. The α-particles were randomly generated in the Hf volume with a mean emission energy of 5.48 MeV. The atomic number of hafnium (72) is much lower than that of americium (95) which is used as an active volume in this study. Americium as an active volume material will attenuate the α radiation more, and therefore, less α-particles will reach the scoring volume, contributing to a decreasing absorbed dose. Additionally, Ramos-Moreira (2020) employed a larger α-particle source (5x5 cm^2) and examined a larger ROI (3.4 cm diameter) compared to the current study, which used a source with a diameter of 5 mm and an ROI with a diameter of 1 mm. Other differences include the activity of the source, which is used for normalization, and as per equation 5.1, it has an impact on the dose rate. All the factors mentioned affect the final dose rate and explain the difference in final dose rate between simulations performed in the current study and published results by Ramos-Moreira (2020).

By comparing the simulation results of the current study with previous research, it is clear that the geometry and materials description of the setup in the simulation toolkit plays an important role in determining the outcomes. As the geometry and composition of the source and film were meticulously modeled and simulated in this study, the presented results can be deemed reliable. The obtained dose rate value in water can be utilized to estimate the absorbed dose in tissue for clinical purposes. Furthermore, the user code used in this study can be extended to other configurations of α-particle emitting sources, radiochromic films, and surrounding media. The dose rate value of 1.096 $\pm$ 0.008 Gy/min was used to convert the different exposure times into doses during the experimental phase of the study.

3.4.2 Film Irradiations

Previous studies have explored α-film dosimetry experimentally using multiple types of films of the EBT model. In a recently published study, El-Naggar *et al.* (2022) [72] irradiated EBT2-M model GafChromic® radiochromic film with an ^{241}Am source at different exposure times with a maximum absorbed dose of 830.7 Gy. The authors used unlaminated film,

Parameters	This work	Ramos-Moreira
Software	Geant4 toolkit ver. 10.02 P2	TOPAS ver. not specified
Source radiation	^{241}Am	α particles ($\bar{E}$=5.48 MeV*)
Source material	Am (Z = 95)	Hf (Z = 72)
Source dimensions	5 mm ⌀ 0.8 nm thick	5×5 cm 1 μm thickness
Gold cover thick	50 nm	2μm
Activity	30.02 kBq (1997)	7.4 MBq (2015)
EBT3 model GafChromic® Film	Unlaminated	Customized**
Scoring material	LiPCDA (14 μm thick)	water (10 μm thick)
	Water (14 μm thick)	
Scorers	Voxels***	Voxels†
ROI [mm ⌀]	∼1	∼34
Statistical uncertainty	Batch method	Variation between scored dose

* $\bar{E}$: Mean energy.
** The protective layer was removed by the vendor and assumed to be unlaminated.
*** Voxel sizes are specified in the methods section.
† Voxel size was not specified.

Table 3.4: Comparison of the input parameters for the MC simulation between this work and published work. For more details regarding published MC results, refer to Ramos [44].

which was composed of a top coat of 5 μm, an active layer of 30 μm, and a bottom polyester substrate base of 175 μm. Unlike the present study, El-Naggar *et al.* (2022) employed a different data analysis approach, which entails fitting the data with an exponential function converting the different color channels to the greyscale levels for each exposure time (in hours). The authors confirmed that the red color channel is the most sensitive, while the blue color channel is the least sensitive. Previous studies [66, 73] have also shown this high sensitivity and low uncertainty of the red channel, which makes it appropriate for lower doses (approximately 8 Gy). However, for the current study, the use of the red channel is not feasible for the high-dose ranges used (up to 1184 Gy), owing to the saturation of the red channel at higher doses. According to Devic *et al.* (2011) [73], for higher doses, the green

channel is recommended since it can provide a smaller uncertainty when the PV_{norm} is used as a response function for higher doses. Thus, the results shown are from using the green channel.

In the current work, unlaminated EBT3 films were irradiated with an ^{241}Am source and 6 MV photons. The response of GafChromic® films will vary depending on the radiation quality used. Regarding α-particles, which are charged with a high LET and create dense ionizations along their tracks, their energy is fully deposited after traveling approximately ∼40-100 μm. However, considering that the active centers in the film's active layer are separated by ∼50 μm, it implies that not all the active centers will be activated by α-particles. This phenomenon is referred to as the quenching effect. The quenching effect is LET-dependent and occurs inside the active layer of the film. When EBT films are exposed to high-LET radiation, the energy deposited per unit area of the film can increase the film polarization, leading to a reduction in sensitivity. This is because the polymerization in the active layer of the film is dependent on the formation of free radicals, and if the density of free radical formation along the particle track becomes higher, then fewer polymerization events occur, causing a loss in signal. As a result, the quenching effect occurs due to the saturation of polymerization sites inside the active layer, leading to an under-response of the film [74, 75]. Photons, on the other hand, are neutral, low-LET radiation that can travel farther distances into the film and generate secondary electrons that can reach the active centers in the active layer of the film.

Upon conducting a more in-depth analysis of the data in this study, the polynomial function presented in equation 3.5 was used to fit the PV_{norm} data. This function was slightly modified from the presently employed function for photon film dosimetry published by Devic *et al.* (2005, 2011, 2016, 2018) [37–40]. Despite the differences between the two radiation qualities, for the current study, it was determined that equation 3.5 was suitable for α-radiation as well. The primary distinction between this function with the previously published function is that the a parameter has been set to zero, which results that the function relying on the exponent of the n parameter 3.5. This fit function was deemed the simplest function to fit the data with since it is a polynomial correction to a linear form. The green channel pixel values fit best to this function since they are increasing linearly with the

dose. In addition, the relative uncertainties of the fitting parameters were lower, indicating a proper fit to the data. Further comparisons between the α and photon radiation calibration curves have indicated that the α has a more linear response as the dose increases due to the value of the n parameter. The n parameter is the exponential component of the fit equation and is determined to be 1.28 $\pm$ 0.02 and 1.33 $\pm$ 0.03 for α-particle and photon radiation, respectively.

Additionally, raw PV $<$ 10 000 which corresponds to absorbed doses above 120 $\pm$ 0.044 Gy, for the green channel was not considered in the data analysis, due to the sensitivity of the flatbed scanner. The flatbed scanner used in this study cannot properly scan high-intensity irradiation regions, therefore the measured response value for raw PV $<$ 10 000 is a result of the scattered light transmitting through the film. Consequently, the measured signal is the scattered light from the scanning system, as well as the inherent noise of the charge-coupled device (CCD) linear detector of the scanner. By discarding these raw PV, the signal is now independent of the transmission of the film. Therefore, any dose above 120 $\pm$ 0.044 Gy cannot appropriately represent response values for the unlaminated EBT3 model GafChromic® film. This analysis indicates that the dose range for α-radiation for unlaminated EBT3 model GafChromic® film can be defined between 0 and 120 $\pm$ 0.044 Gy for the green color channel. This differs from the stated optimal dose range for photons of 0.1 cGy to 10 Gy.

Furthermore, looking at figure 3.7a, the PV_{norm} increases faster with an increasing dose for α-particles compared to photons. Therefore, the PV_{norm} film response indicates that α-particles produce a lower response in the film than photons since photons activate each active center in the active layer of the film, i.e. the quenching effect. Nevertheless, the PV_{norm} difference between α-particles and photons are not statistically significant (p = 0.586). By removing the high doses from the analysis, the two calibration curves (α and 6 MV photon beam) can be compared indicating that α-particles' energy deposition leads to higher absorbed doses in the EBT3 model GafChromic® film compared to photons [76].

In future research, it may be necessary to investigate the film responses to α-radiation at doses exceeding 120 $\pm$ 0.044 Gy. If such an investigation is deemed necessary, an alternative type of film such as HD-V2 model film could be employed. This alternative film has shown

promise in previous studies for its ability to accurately measure radiation doses in high-dose applications [77]. Therefore, further research could explore the use of HD-V2 film in the context of high-dose α-radiation measurements, in order to improve the accuracy and reliability of these measurements and enhance our understanding of the effects of α-radiation exposure.

3.5 Conclusion

In this work, the response of the unlaminated EBT3 model GafChromic® film to α-radiation using an ^{241}Am source was studied by means of MC simulations and experimental measurements. Using the Geant4 simulation toolkit, the dose rate for the film was obtained and used to convert exposure times into delivered dose to create dose-calibration curves for α-particle dosimetry. The MC simulations were successfully developed and the calculated dose rates were 1.096 $\pm$ 0.008 Gy/min and 1.113 $\pm$ 0.006 Gy/min for the active layer of the film and water, respectively. The unlaminated EBT3 model GafChromic® film response is reliable for α-irradiation up to 120 $\pm$ 0.044 Gy and was compared with conventional photon film dosimetry. The implemented user code and experimentation can be applied to any other configurations of α-particle emitting sources, radiochromic films, and surrounding media.

3.6 References

1. J. Sorriaux et al., Evaluation of Gafchromic® EBT3 films characteristics in therapy photon, electron and proton beams, Physica Medica **29**, 599 – 606 (2013).
2. W. McLaughlin and L. Chalkley, Measurement of Radiation Dose Distributions with Photochromic, Radiology **84**, 124 – 125 (1965).
3. S. Devic, J. Seuntjeans, E. Sham, and E. B. Podgorsak, Precise Radiochromic Film Dosimetry Using a Flat-bed Document Scanner, Med. Phys. **32**, 2245 – 2253 (2005).
4. R. Dreindl, D. Georg, and M. Stock, Radiochromic film dosimetry: Considerations on precision and accuracy for EBT2 and EBT3 type films, Zeitschrift für Medizinische

Physik **24**, 153–163 (2014).

5. S. Khachonkham et al., Characteristic of EBT-XD and EBT3 radiochromic film dosimetry for photon and proton beams, Phys. Med. Biol. **63** (2018).
6. M. Martisikova, B. Ackermann, and O. Jackel, Analysis of Uncertainties in Gafchromic EBT Film Dosimetry of Photon Beams, Phys. Med. Biol. **53**, 7013 – 7027 (2008).
7. K.-H. Lee, J.-Y. Shin, and E.-H. Kim, Measurement of activity distribution in an Am241 disc source using peeled-off Gafchromic EBT3 films, Appl. Radiat. Isotopes **135**, 192 – 200 (2018).
8. A. G. D. Films, Gafchromic EBT.
9. S. Devic, Radiochromic Film Dosimetry: Past, present, and future, Euro. J. Med. Phys **27**, 122 – 134 (2011).
10. S. Devic, N. Tomic, and D. Lewis, Reference Radiochromic Film Dosimetry: Review of Technical Aspects, Euro. J. Med. Phys **32**, 541 – 556 (2016).
11. S. Aldelaijan and S. Devic, Comparison of Dose Response Functions for EBT3 model Gafchromic Film Dosimetry, Euro. J. Med. Phys **49**, 112 – 118 (2018).
12. R. Castriconi et al., Dose-response of EBT3 radiochromic films to proton and carbonion clinical beams, Phys. Med. Biol. **62** (2017).
13. S. Poty et al., α-Emitters for Radiotherapy: From Basic Radiochemistry to Clinical Studies-Part 1, J. Nucl. Med. **6**, 878 – 884 (2018).
14. S. Poty et al., -Emitters for Radiotherapy: From Basic Radiochemistry to Clinical Studies-Part 2, J. Nucl. Med. **7**, 1020 – 1027 (2018).
15. J. Pouget and J. Constanzo, Revisiting the Radiobiology of Targeted Alpha Therapy, Frontiers in Medicine 8, 1020 – 1027 (2021).
16. N. Tafreshi et al., Development of Targeted Alpha Particle Therapy for Solid Tumors, Molecules **24** (2019).
17. S. Navalkissoor and A. Grossman, Targeted Alpha Particle Therapy for Neuroendocrine Tumours: The Next Generation of Peptide Receptor Radionuclide Therapy, Neuroendocrinology **108**, 256 – 264 (2019).
18. A. I. Kassis, Therapeutic Radionuclides: Biophysical and Radiobiologic Principles, **38**, 358 – 366 (2008).

19. A. S. Mustaquim, S. Kandaiya, N. N. A. Razak, and N. Z. Yahaya, The Gafchromic EBT3 film as alpha detector, J. Phys.: Conf. Ser. **1083**, 12 – 19 (2018).
20. C. Ng et al., Quality assurance of alpha-particle dosimetry using peeled-off Gafchromic EBT3® film, Radiation Physics and Chemistry **125**, 176–179 (2016).
21. B. Mukherjee et al., A unique alpha dosimetry technique using Gafchromic EBT3® film and feasibility study for an activity calibrator for alpha-emitting radiopharmaceuticals, Brit. J. Radiol. **88** (2015).
22. S. Agostinelli et al., Geant4—a simulation toolkitt, Nuclear Instruments and Methods in Physics Research Section A **503**, 250–303 (2003).
23. H. Moreira, Investigating the mechanisms of α-particle therapy in prostate cancer, (2020).
24. V. Ivantchenko, Electromagnetic Physics: Geant4 Advanced Course.
25. Geant4, Book For Application Developers.
26. E. Mendoza, D. Cano-Ott, P. Romojaro, V. Alcayne, P. G. Abia, V. Pesudo, and R. S. L. Romero, Neutron production induced by -decay with Geant4, Nuclear Instruments and Methods in Physics Research Section A: Accelerators, Spectrometers, Detectors and Associated Equipment **960** (2020).
27. I. Sechopoulos, D. W. O. Rogers, M. Bazalova-Carter, W. E. Bolch, E. C. Heath, M. F. McNitt-Gray, J. Sempau, and J. F. Williamson, RECORDS: improved Reporting of montE CarlO RaDiation transport Studies: Report of the AAPM Research Committee Task Group 268, Med. Phys. **45** (2017).
28. D. R. A. of Canada, Digital Research Alliance of Canada.
29. J. Bar o, J. Sempau, J. M. Fern andez-Varea, and F. Salvat, PENELOPE: An algorithm for Monte Carlo simulation of the penetration and energy loss of electrons and positrons in matter, Nuclear Inst. and Methods in Physics Research B , 31.
30. N. I. of Standards and Technology, X-ray Transition Energy Database.
31. I. A. E. Agency, IAEA - Nuclear Data Section.
32. FLUKA, Introduction to the Monte Carlo simulation of radiation transport.
33. A. F. Bielajew, Fundamentals of the Monte Carlo method for neutral and charged particle transport, (2001).

34. S. Devic, J. Seuntjens, G. Hegyi, E. Podgorsak, C. Soares, A. Kirov, I. Ali, J. Williamson, and A. Elizondo, Dosimetric properties of improved GafChromic films for different digitizers, Med. Phys. **31**, 2392 – 2401 (2004).
35. G. F. Knoll, Radiation Detection and Measurement, John Wiley Sons, Inc., 2000.
36. D. Demir, M. Eroglu, and A. Tursucu, Studying of characteristics of the HPGe detector for radioactivity measurements, Joirnal Of Instrumentation **8** (2013).
37. X-ray Spectroscopy with PIN diodes, volume 857.
38. E. B. Podgorsak, Radiation Physics for Medical Physicists, volume 3, Springer International Publishing Switzerland, 2016.
39. L. Arazi, T. Cooks, M. Schmidt, Y. Keisari, and I. Kelson, Treatment of solid tumors by interstitial release of recoiling short-lived alpha emitters, Phys. Med. Biol. **52**, 5025 – 5042 (2007).
40. T. Cooks, L. Arazi, M. Schmidt, G. Marshak, I. Kelson, and Y. Keisari, Growth retardation and destruction of experimental squamous cell carcinoma by interstitial radioactive wires releasing diffusing alpha-emitting atoms, Int. J. of Cancer **122**, 1657 – 1664 (2008).
41. T. Cooks, M. Schmidt, H. Bittan, E. Lazarov, L. Arazi, I. Kelson, and Y. Keisari, Local control of lung derived tumors by diffusing alpha-emitting atoms released from intratumoral wires loaded with radium-224, Int. J. Radiat. Oncol. Biol. Phys. **74**, 966 –973 (2009).
42. T. Cooks, M. Tal, S. Raab, M. Efrati, S. Reitkopf, E. Lazarov, R. Etzyoni, M. Schmidt, L. Arazi, I. Kelson, and Y. Keisari, Intratumoral Radium-224 Loaded Wires Spread Alpha-Emitters Inside Solid Human Tumors in Ahtymic Mice Achieving Tumor Control, Anticancer Res. **32**, 5315 – 5322 (2012).
43. L. Arazi, Thesis; Diffusing Alpha-Emitters Radiation Therapy: Theoretical and Experimental Dosimetry, pages 1–285 (2008).
44. K. Lee, U. Lee, and E. Kim, A practical alpha particle irradiator for studying internal alpha particle exposure, Appl. Radiat. Isotopes **115**, 304 – 311 (2016).
45. H. El-Naggar, E. Ghanim, M. E. Ghazaly, and T. Salama, On the reigstration of low energy alpha particle with modified GafChromic EBT2 radiochromic film, Rad. Phys.

and Chem. .

46. S. Devic, Radiochromic Film Dosimetry: Past, present and future, Euro. J. Med. Phys **27**, 122 – 134 (2011).
47. J. B. Marion and M. L. Roush, The Effects of Nuclear Radiations, volume 2, Academic Press, Inc., 1974.
48. A. Aydarous and M. E. Ghazaly, Characterization of HD-V2 Gafchromic Film for Measurement of Spatial Dose Distribution from Alpha Particle of 5.5 MeV, Int. J. Physical Math. Sciences.

3.7 Author contributions statement

The contribution of each author to this manuscript was the following. Victor Diaz developed a Geant4 user code to simulate the decay, detailed geometry, materials, and composition of the radioactive ^{241}Am source and the unlaminated GafChromic® EBT3 film. Victor Diaz analyzed the results with a Matlab script that he developed from scratch and was involved in the experimental phase by conducting part of the film irradiations and subsequent scanning procedures. Mélodie Cyr performed and analyzed the experimental measurements. Mélodie completed all film irradiations with the ^{241}Am source and scanned the films according to the appropriate protocol. Mélodie analyzed the scanned .tiff files with an in-house Python script that was modified to complete new necessary film calculations. Mélodie analyzed the uncertainties according to the propagation of uncertainty rules and the methods previously described by Dr. Devic. Dr. Slobodan Devic shared his expertise in EBT photon-based film dosimetry, besides useful comments regarding the manuscript, Nada Tomic helped Victor and Mélodie with the film measurements. Dr. David F. Lewis provided accurate dimensions and composition of the GafChromic® EBT3 films and shared his experience on radiochromic film dosimetry. Dr. Shirin A. Enger provided a preliminary version of the Geant4 user code which was modified according to the needs of the experiment and provided continuous and valuable feedback on this manuscript.

3.8 Additional information

Competing interests The authors declare no competing interests.

Acknowledgments This research was conducted as part of the activities of MEDTEQ+, thanks to the financial support of the Ministry of Economy and Innovation - PSOv2b program, cofounded with TransMedTech (Canada First Research Excellence Fund), Mitacs, the MUHC Foundation, and Alpha Tau Medical. The work was also supported by the Canada Research Chairs Program. Victor Diaz acknowledges funding the Mexican institution Consejo Nacional de Ciencia y Tecnología (CONACyT) for granting him the CONACyT-Regional Centro 2020' scholarship to pursue graduate studies at McGill University, Canada. Computations were performed on the Cedar cluster of the Digital Research Alliance of Canada.

Bridging Text

It was mentioned earlier that DaRT is of great interest in α-based dosimetry due to its great potential and thus, a robust dosimetry protocol is required. Examples of this dosimetry include film and *in-vivo* dosimetry.

The previous manuscript covered a study of the response of the unlaminated GafChromic® EBT3 film to α radiation to develop a dose-calibration protocol for α-particle dosimetry. In this work, an α-particle emitting source (^{241}Am) was used for both the simulations and experimental measurements. However, this study is not limited to ^{241}Am sources, the DaRT technique can also be studied using these types of radiochromic films. As it was stated in this manuscript, GafChromic® EBT films are important because of their high level of accuracy for dose values between 0.1-1000 Gy, their high spatial resolution, low energy dependence, etc., and that any type of experimental measurements with this radiochromic film must be benchmarked with MC simulations.

Therefore, in order to study the response of the unlaminated GafChromic® EBT3 films to the type of radiation emitted from DaRT seeds, it is important to reproduce the diffusive behavior of the radioactive daughters in the MC -based user-code. The following manuscript addresses this subject since in this work the main aim was to implement a method to distribute the diffusive daughters around the DaRT seed according to reported experimental data, and observe the dose distribution. This user code will not only allow us to study the response of unlaminated GafChromic® EBT3 films but also to study the response of different types of detectors destined for *in-vivo* dosimetry and quality control (QA) for DaRT.

Both studies can be extended to other configurations of α-particle emitting sources, environment, and detectors by merging the two user codes. This merging will result in a broader user code that will allow the user to select any type of desired configuration and corroborate experimental data.

Chapter 4

Body of Thesis

^{220}Rn and ^{212}Pb distribution from radioactive seeds in Diffusing alpha-emitters Radiation Therapy (DaRT)

Victor D. Diaz-Martinez[1,3], Liam Carroll[1,3], Slobodan Devic[1,3], Shirin A. Enger[1,2,3]

[1]Medical Physics Unit, Department of Oncology, Faculty of Medicine, McGill University, Montreal, Québec, Canada. [2]Research Institute of McGill University Health Centre, Montreal, Québec, Canada. [3]Lady Davis Institute for Medical Research, Jewish General Hospital, Montreal, Québec, Canada.

Abstract

Background: A novel brachytherapy treatment, called Diffusing alpha-emitter Radiation Therapy (DaRT) delivers a lethal dose of radiation to the tumor while sparing healthy tissues. DaRT consists of ^{224}Ra atoms fixed to the surface of the seed that α-decay releasing other α-emitting daughters. These daughters diffuse between the cancerous cells

allowing α-particles to deposit their energy up to a few mm from the source. Currently, there is a lack of an α-based dosimetry software that can simulate this environmental diffusion and score the absorbed dose in the surrounding medium.

Purpose: The aim of this study was to develop a Monte Carlo-based user code to obtain the energy spectra emitted from the ^{224}Ra decay and its daughters and score the interaction of the decay products with the matter. This was done through the implementation of the environmental diffusion of ^{220}Rn and ^{212}Pb based on the solution of their respective diffusion equations. The developed user code can be used to investigate DaRT dosimetry and aid in the development of radiation detectors for acceptance testing of the applicators, quality assurance, and in-vivo dosimetry.

Methods: For this study, a Monte Carlo-based user code built on the Geant4 simulation toolkit was developed to model and simulate a stainless steel DaRT seed (0.4 mm inner diameter and 0.7 mm outer diameter) with 1×10^{8} ^{224}Ra atoms randomly sampled on the surface of the seed to obtain the energy spectra of the emitted source. One million ^{224}Ra atoms were simulated to distribute the ^{220}Rn and ^{212}Pb atoms around the seed according to their respective diffusion equations solutions. Only the alpha particles were considered for this second simulation. The dose distribution around the seed was determined by means of scoring the dose inside small voxels. The results from the simulation were analyzed with another in-house Matlab script (version R2021a).

Results: The energy spectra obtained from the simulated ^{224}Ra decay were found to be in good agreement with reported values within acceptable percentage difference ranges 0.006-0.015% for α-particles, 0.179 -4.812% for the β-particle energy spectra, and 0.081% for γ-photons. As for the distribution of the diffusive daughters, the dose distribution map showed that the contribution of α-particles due to diffusion can reach a further distance from the surface of the seed.

Conclusions: The developed Geant4-based user code allowed the distribution of the

diffusive daughters around the DaRT seed obtaining the extension at which α-particles can deposit their energy.

4.1 Introduction

In radiotherapy, ionizing radiation is used to cause irreparable damage to the DNA and inhibit cell cycling of the cancer cells. However, radiation does not just cause selective damage in cancerous cells but also injures healthy tissue. Many strategies have been developed for delivering doses in radiotherapy to maximize the effect of radiation on tumor cells and to spare the surrounding healthy tissues. Conventional brachytherapy, a form of radiotherapy where radiation is administered from radiation sources (seeds) placed directly into or near the tumor, is one of the strategies. The steep dose gradient from brachytherapy sources results in an improved therapeutic ratio compared with external beam radiotherapy for selected tumor sites. In addition to photon emitting brachytherapy sources, several β-emitting sources are also used such as ^{106}Ru [7] for treatment of uveal melanoma or ^{90}Sr/^{90}Y used in intravascular brachytherapy [8, 9]. However, brachytherapy was first introduced by using the α-emitting radionuclide ^{226}Ra after its discovery by Marie Klodowska–Curie and Pierre Curie. Interstitial radium therapy was proposed by Bell in 1903 [78]. Table 4.1 shows the most used brachytherapy sources with their respective mode(s) of decay and their half-life. Radionuclides emitting γ or β-radiation is associated with low linear energy transfer (LET) and consequently low relative biological effectiveness (RBE). α-particles on the other hand, have an LET $\sim$ 100 times greater than γ or β-radiation and hence, a higher RBE.

There have been a number of α-emitting radionuclides considered for targeted therapy application for the treatment of micro-metastatic disease due to the short range of emitted α-particles. In addition, only a limited number are realistically available due to either a too-short or too-long half-life, a lack of realistically viable chemistry, complicated decay pathways, or actual production/availability issues [79].

4.1.1 Diffusing alpha-emitters Radiation Therapy Technology

Recently, a novel brachytherapy treatment option for solid tumors is offered through alpha-emitters released from ^{224}Ra-loaded seeds [16, 17, 22, 23, 25–28, 80, 81]. This novel

Radionuclide	Decay mode	Half-life
^{131}Cs	Electron Capture (ϵ)	9.7 days
^{137}Cs	β^- and γ-rays	30.17 years
^{60}Co	β^- and γ-rays	5.26 years
^{90}Sr	β^-	28.79 years
^{90}Y	β^- and γ-rays	2.7 days
^{192}Ir	γ-rays	73.8 days
^{125}I	Electron Capture (ϵ)	59.6 days
^{103}Pd	Electron Capture (ϵ)	17.0 days
^{106}Ru	β^-	1.02 years
^{226}Ra	α	1599 years

Table 4.1: List of the radionuclides most used in brachytherapy with their respective modes of decay and their half-lives. This table was adapted from [10]

technique is called diffusing alpha-emitters radiotherapy (DaRT) and delivers a lethal dose of radiation to the tumor while sparing nearby radiation-sensitive healthy tissues due to the short range of alpha particles in tissue. DaRT consists of ^{224}Ra atoms ($t_{1/2}$ = 3.66 days) fixed to the surface of brachytherapy seeds that emits high-energy α-particles during its decay. Once the ^{224}Ra has α-decayed, it transforms into the short-life daughter ^{220}Rn, which by recoil is released from the seed. This radionuclide will also α-decay, but since it is a noble gas, it will diffuse between the extra- and intra-cellular space [16, 28]. The ^{220}Rn diffusion will extend the distance at which α-particles can deposit their energy in the medium. This distance can be further extended due to the diffusion of ^{212}Pb by means of lead-binding proteins. Given that this radionuclide decays into other α-decaying daughters, the diffusion of ^{220}Rn and ^{212}Pb overcome the short range of α-particles in tissue (<100 μm) contributing to a high-dose region up to few mm around the source [16, 80]. Figure 4.1 shows the decay scheme of ^{224}Ra from which the mean energy of the α-particles emitted during the decay is indicated. From this figure, it can be seen that one decay of ^{224}Ra contributes with 5 α-particles throughout the decay chain.

The distance at which ^{220}Rn atoms diffuse depends on the effective diffusion length given by the following equation provided by Arazi L. *et al.* (2007) [16]:

$$L_{Rn} = \sqrt{\frac{D_{Rn}}{\lambda_{Rn} - \lambda_{Ra}}} \tag{4.1}$$

where D_{Rn} is the *effective diffusion coefficient* of ^{220}Rn in tissue, and the λs are the

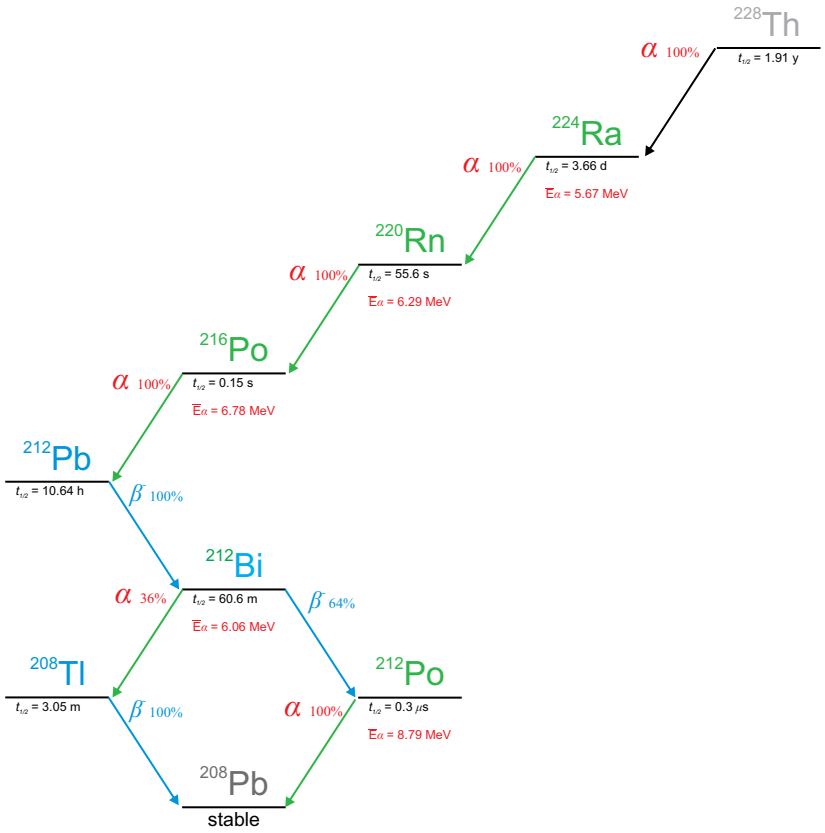

Figure 4.1: Scheme of the decay chain of ^{224}Ra showing each daughter's emissions and their respective energies and probabilities (where applicable). All the α-decaying radionuclides used in DaRT seeds are shown in green while the β-decaying daughter are indicated in blue. ^{212}Bi is shown in blue and green because it can either α or β decay. ^{228}Th is indicated in gray as it is the generator of ^{224}Ra.

decay constants of ^{220}Rn (λ_{Rn}) and ^{224}Ra (λ_{Ra}). Equivalently, the diffusion length for ^{212}Pb is given by the following equation:

$$L_{Pb} = \sqrt{\frac{D_{Pb}}{\lambda_{Pb} + \alpha_{Pb} - \lambda_{Ra}}} \tag{4.2}$$

Where D_{Pb} is the *effective diffusion coefficient* of ^{212}Pb in tissue, α_{Pb} is the leakage rate coefficient, and λ_{Pb} and λ_{Ra} are the decay constants of Lead and Radium, respectively. This group provides two reference values for the effective diffusion coefficient: D_{Rn} : $1.9 \times 10^{-5} cm^2 s^{-1}$, and D_{Rn} : $0.5 \times 10^{-5} cm^2 s^{-1}$ which yield two diffusion lengths of 0.39 mm and 0.20 mm, respectively. As for ^{212}Pb, experimental diffusion length values of approximately 0.8 mm obtained from tumor histologies are reported in the literature [28]. Hence, the diffusion length of ^{220}Rn and ^{212}Pb determine the spatial distribution of the diffusing atoms, and therefore the distance at which α-particles can deposit their energy. However, these

diffusion lengths vary for different tumor types between patients.

4.1.2 Monte Carlo Method

DaRT is a new treatment modality in need of new dosimetry standards and the development of radiation detectors for acceptance testing of the applicators, quality assurance, and *in-vivo* dosimetry. This can be done by the Monte Carlo method, which has been used in different areas of medical radiation physics for over 50 years and triggered innovations in this domain [82]. Improved description of radiation transport models and cross sections in the radiotherapy energy regime as well as the optimization of the computing systems have contributed to its wider use. Dosimetric applications in radiotherapy span from targeted radionuclide therapy to treatment planning radiation dose distribution in heterogeneous media for external beam radiotherapy and brachytherapy.

The Monte Carlo codes currently available are MCNP5 [83] EGSnrc [84], Geant4 [46], FLUKA [85], PENELOPE [86]. We have chosen to work with Geant4 since it is a flexible and open-source software toolkit for simulating the passage and interaction of charged and neutral particles with matter. The physics processes implemented in Geant4 cover electromagnetic, hadronic, and optical processes, a large set of long-lived particles, materials, and elements, over a wide energy range from 250 eV to the TeV. The toolkit has an object-oriented design which allows it to accommodate a large variety and alternative physics models and cross sections [46]. However, in Geant4 and other Monte Carlo codes, when ^{224}Ra decays, all its daughters in the decay chain are created in the same position as the mother radionuclide and no change in the position due to environmental diffusion occurs.

4.1.3 Aim

The aim of this study was to develop a Monte Carlo-based Geant4 user code to obtain the energy spectra emitted from ^{224}Ra decay and its daughters, transport and score the interaction of the decay products with matter as well as add the environmental diffusion of the ^{220}Rn and ^{212}Pb based on experimental studies [28]. This user code can be used to investigate DaRT dosimetry and aid in the development of radiation detectors for acceptance testing of the applicators, quality assurance, and in-vivo dosimetry.

4.2 Methods

4.2.1 DaRT source characteristics

The DaRT seeds consist of a hollow stainless steel (density 7.92 g/cm^3) cylinder with an inner and outer radius of 0.2 mm and 0.35 mm respectively [16], with variable length. In this study, we have simulated a 10 mm long seed as shown in figure 4.2a. According to the specifications for this technology, the ^{224}Ra atoms are fixed on the surface of the seed through the following process. ^{224}Ra atoms are produced from the decay of ^{228}Th, known as the *^{228}Th generator*, which consists of a surface covered with a thin layer of ^{228}Th atoms placed at 5-15 mm away from a collecting wire (seed). This wire is held at a negative potential (2-3 kV) to collect the released ^{224}Ra atoms by recoil from the surface. Finally, the wire is heated and immersed in water to fix the ^{224}Ra atoms to its surface [16]. Once these ^{224}Ra atoms are fixed, they *alpha*-decay into ^{220}Rn atoms which are emitted from the seeds' surface by recoil as illustrated by figure 4.2b).

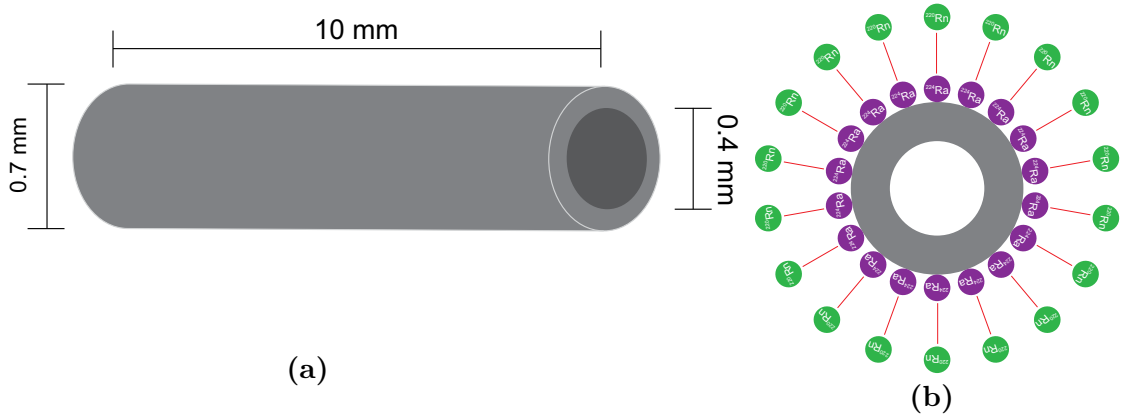

Figure 4.2: Dimensions of the stainless steel 316LVM seed (a) and a representation of the emission of the ^{220}Rn atoms (green) emitted by recoil from the ^{224}Ra atoms (purple) fixed to the seed's surface.

4.2.2 Monte Carlo Simulations

An in-house Monte Carlo-based user code built on the Geant4 (Version 10.7 Patch-02) simulation toolkit [46] was developed to perform two sets of simulations. The first set was used to simulate the entire decay chain of ^{224}Ra and obtain the emitted energy spectra

from the seed for comparison with the measured reported database. The second set of simulations was performed by simulating only the emitted α-particles from the decay to compare with published work. The main objective of this second set of simulations was to transport the diffusive daughters in water and score the interactions of the emitted radiation around the seed.

In order to perform these simulations the DaRT seed was modeled as described in figure 4.2a according to the specifications from the vendor (Alpha Tau Medical Ltd.) inside a 20 cm radius water sphere. 1×10^{8} ^{224}Ra atoms were randomly sampled to isotropically decay on the surface of the simulated seed to achieve an uncertainty less than 1% for the majority of the emitted energy spectra and an uncertainty less than 5% for other cases. Additionally, 1×10^{6} ^{224}Ra atoms were simulated, but only taking into account the α-particles emitters to assess and compare the extension of the dose around of the seed. Only one million particles were simulated due to computational time. The nuclear decay of the radionuclide was explicitly simulated by means of Geant4 radioactive decay physics packages, where the radioactive decay data was taken from the Evaluated Nuclear Structure Data File (ENSDF) [87]. This eliminates the need to include hard-coded decay energy spectra for ^{224}Ra and its daughter in the decay chain. The interactions of the α-particles with the medium in the simulations were handled through the G4EmStandardPhysics_option3 package which is used for proton and ion therapy [58, 59], and uses stopping powers from the International Commission on Radiation Units and Measurements (ICRU) 49 report [60]. A production cutoff of 50 μm was defined for secondary particles. In accordance with the recommendations of the American Association of Physicists in Medicine Task Group 268 report [61], all the input parameters used the simulation are presented in table 4.2. The simulations were performed on the Cedar cluster of Digital Research Alliance of Canada [62].

Item	Description	References
Toolkit	Geant4 version 10.02 P2	Agostinelli *et al* [46]
Cross-sections	Penelope Stopping powers database (ICRU49)	Barol *et al* [63] Mendoza *et al* [60].
Validation	The ^{224}Ra energy spectra were compared to the reported values from the IAEA databases. The maximum distribution length was compared to the effective diffusion length defined as the maximum limit for this study	IAEA Live Chart of Nuclides [56] Arazi L. *et al.* [16]
Source description	Hollow stainless steel cylinder with ^{224}Ra atoms distributed on the surface	Arazi L. *et al.* [16]
Production Cut-off for all particles	30 μm	
Statistical uncertainty	History-by-history method for the simulations and percentage difference for the simulated energy spectra.	FLUKA [64], A. F. Bielajew [65]

Table 4.2: Summary of parameters used for Monte Carlo simulation

The Positioning Method

It was previously mentioned that Geant4 generates all the products in the decay chain of ^{224}Ra, however, it does not simulate the environmental diffusion of ^{220}Rn and ^{212}Pb. In this study, ^{220}Rn and ^{212}Pb were distributed around the seed in a two-step process. The first step consisted of numerically solving the diffusion equations of ^{220}Rn and ^{212}Pb (equations 4.3 and 4.4) using an in-house Matlab script. The results of the diffusion equations were

converted into a probability distribution and stored in a text file that was later used as input to the Geant4 user code. The second step consisted of distributing the diffusive atoms around the seed according to the results stored in the text file, this method was named the *'positioning method'*. According to figure 4.1, the daughter of ^{220}Rn: ^{216}Po, has a very short half-life such that it is considered to be generated and decays in the same point as ^{220}Rn [16]. Thus, the implemented method does not affect the position of ^{216}Po or any other non-diffusive daughter, but the positions of ^{220}Rn and ^{212}Pb by transporting them up to a different position from the seed's surface. Figure 4.3 shows a general workflow of this method.

$$\frac{\partial n_{Rn}}{\partial t} = D_{Rn}\left(\frac{1}{r}\frac{\partial}{\partial r}\left(r\frac{\partial n_{Rn}}{\partial r}\right) + \frac{\partial^2 n_{Rn}}{\partial z^2}\right) - \lambda_{Rn} n_{Rn} \tag{4.3}$$

$$\frac{\partial n_{Pb}}{\partial t} = D_{Pb}\left(\frac{1}{r}\frac{\partial}{\partial r}\left(r\frac{\partial n_{Pb}}{\partial r}\right) + \frac{\partial^2 n_{Pb}}{\partial z^2}\right) + \lambda_{Rn} n_{Rn} - (\lambda_{Pb} + \alpha_{Pb}) n_{Rn} \tag{4.4}$$

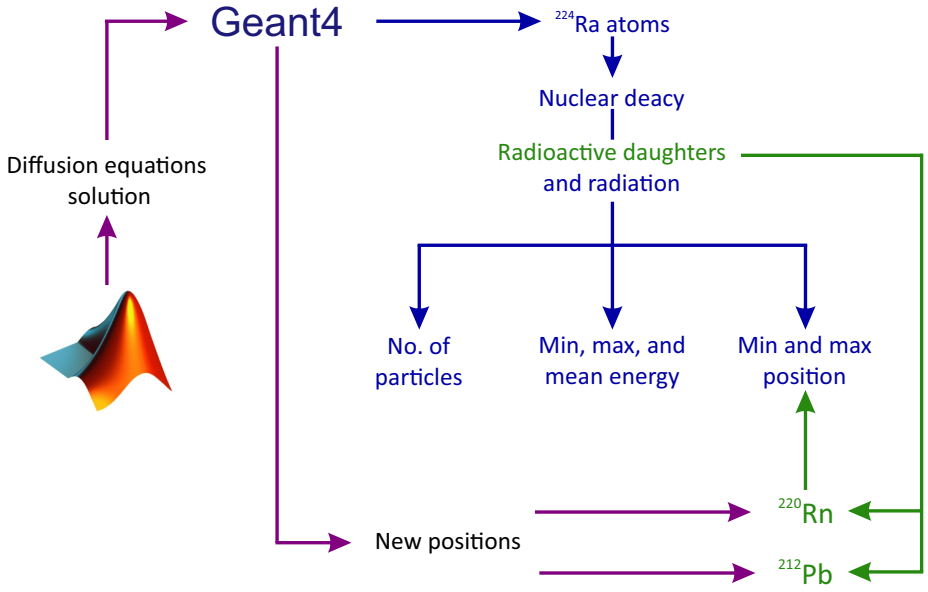

Figure 4.3: Workflow of the *'positioning method'*. Geant4 generates the ^{224}Ra atoms on the surface of the seed simulating their nuclear decay. From this decay, information such as the number of generated decay products, energy, and position was retrieved. Geant4 also uses the Matlab-generated text file with the solution to the diffusion equations to distribute the diffusive daughters and retrieve their new positions for comparison.

In order to verify the performance of the implemented method, and therefore, the dose distribution, a voxelized scoring volume was placed around the seed to score the dose. This scoring volume was divided into $500 \times 500 \times 80$ voxels, each one defined as a scoring volume of $0.1 \times 0.1 \times 0.1\ mm^3$. Different dose maps were obtained at different distances from the center of the seed (from -4 mm to 3 mm) along the z-axis of the simulated world. These dose maps were used to assess the distance at which α-particles can deposit their energy in the x,y, and z directions. The results of both sets of simulations such as the decay chain per event, total number of particles, energy, and position were scored within the Geant4 user code. Display of the energy spectra of the decay chain data and the dose distribution around the seed was handled using an in-house Matlab script (version R2021a).

4.3 Results

The results for these simulations reported in this work include the α, β, and photon energy spectra of the source, and the dose distribution around the seed at different distances.

4.3.1 Energy Spectra emitted from the ^{224}Ra source

One way to validate the developed user code was by scoring the decay products from the entire ^{224}Ra decay chain. For this purpose, the α (figure 4.4a), β (figures 4.4b, 4.4c, and 4.4d), and γ (figure 4.4e) energy spectrum were obtained from the simulation. The energy spectra were normalized to their respective maximum value and finally compared to values reported by the IAEA Live Chart of Nuclides [56]. For the α-particle energy spectrum, only α-particles with energies of relatively high-intensity (labeled in figure 4.4a indicated in figure 4.1) were compared to reported values and were found to be in good agreement within a 0.006-0.015% difference range. As illustrated in 4.1, three β-particle energy spectra are produced in the decay chain, i.e., ^{212}Pb, ^{212}Bi, and ^{208}Tl which were found to be in good agreement with a 4.812%, 0.179%, and 0.240% percentage difference, respectively. These three energy spectra are shown in figure 4.4 and compared with their respective reported energy spectrum obtained from IAEA [56] shown as a red solid line. As for the γ-energy spectrum, the three main relative high-intensity γ peaks shown in figure 4.4e were compared to the IAEA database and were also found to be in good agreement having a percentage difference range up to 0.081%.

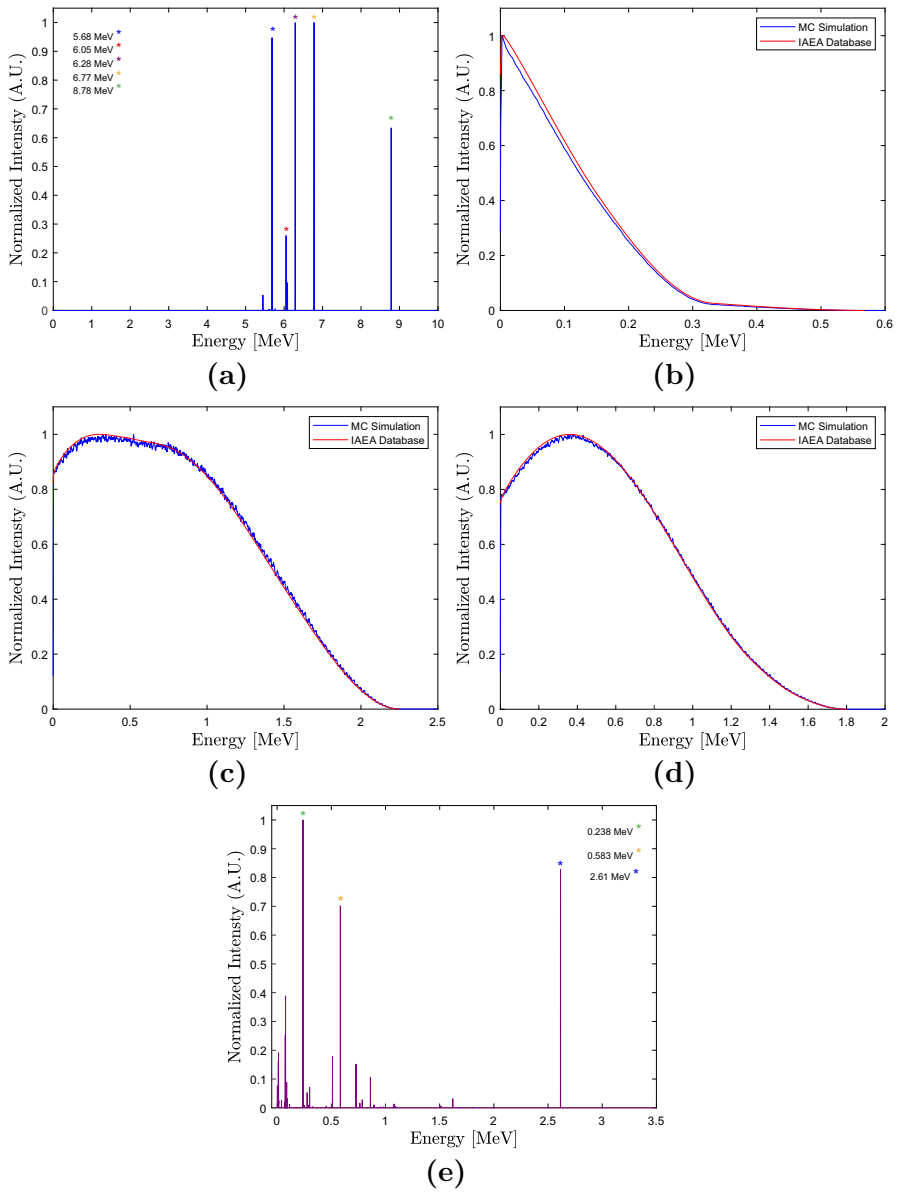

Figure 4.4: Normalized energy spectra of (a) α-particles and β-particles: (b) ^{212}Pb (c) ^{212}Bi, (d) ^{208}Tl, and (e) photons produced during the decay of ^{224}Ra. (a) and (e) show the energies of their respective relative high-intensity radiation. Comparison with data from IAEA is not shown for these plots due to the good agreement. Figures b-d show the simulated energy spectra (blue solid line) compared to reported data from the IAEA (red solid line).

4.3.2 The Positioning method results

The geometry and the distribution of the ^{220}Rn atoms around the DaRT seed are illustrated in figure 4.5. Figure 4.5a shows two concentric circles that correspond to the

hollow DaRT seed viewed from one of its basis and the α-particles distributed around it. The blue lines located on the surface of the seed represent the tracks of the α-particles emitted from the mother (^{224}Ra), and the ones around the seed were emitted from the daughter ^{220}Rn. This visualization does not include the other diffusive daughter ^{212}Pb given that this radionuclide is not an α-particle emitter, but β-decays into an α-emitter daughter. For visualization purposes, only the decay of ^{224}Ra and ^{220}Rn were considered in figures 4.5a and 4.5b. All these emissions were distributed according to the solution of their respective diffusion equations.

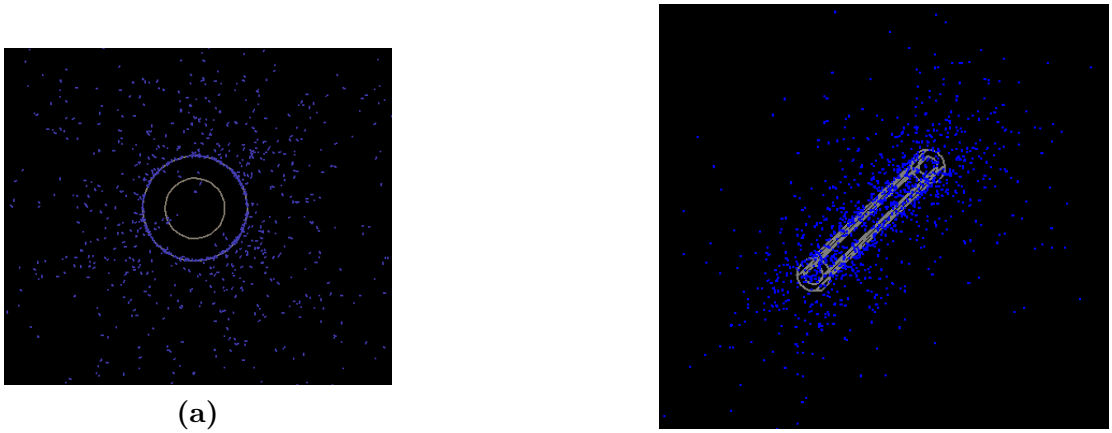

(a) **(b)**

Figure 4.5: Visualization of ^{224}Ra atoms on the surface of the seed and the distribution of the ^{220}Rn atoms showing their respective α-emissions viewed from the basis of the seed (a) and a general view of the seed with the α-particles around it (b).

The contribution of only α-particles to the absorbed dose due to the diffusion was evaluated by means of dose maps shown in figure 4.6. These dose maps were obtained at different distances over the z-direction indicated on top of each one of them. These dose maps show a decrease in the absorbed dose as a function of the distance indicated in each color bar, having the highest dose values at z = 0 mm (at the center of the seed's plane). Each dose map shows a red rectangle in the center representing the geometry of the seed. The red rectangle was used to observe the dose distribution in relation to the seed surface at different distances. It can be seen that in the x,y, and z directions, the dose values as a function of the distance are dramatically reduced at distances as of $\sim$3 mm. This can also be observed in Heger's work [88].

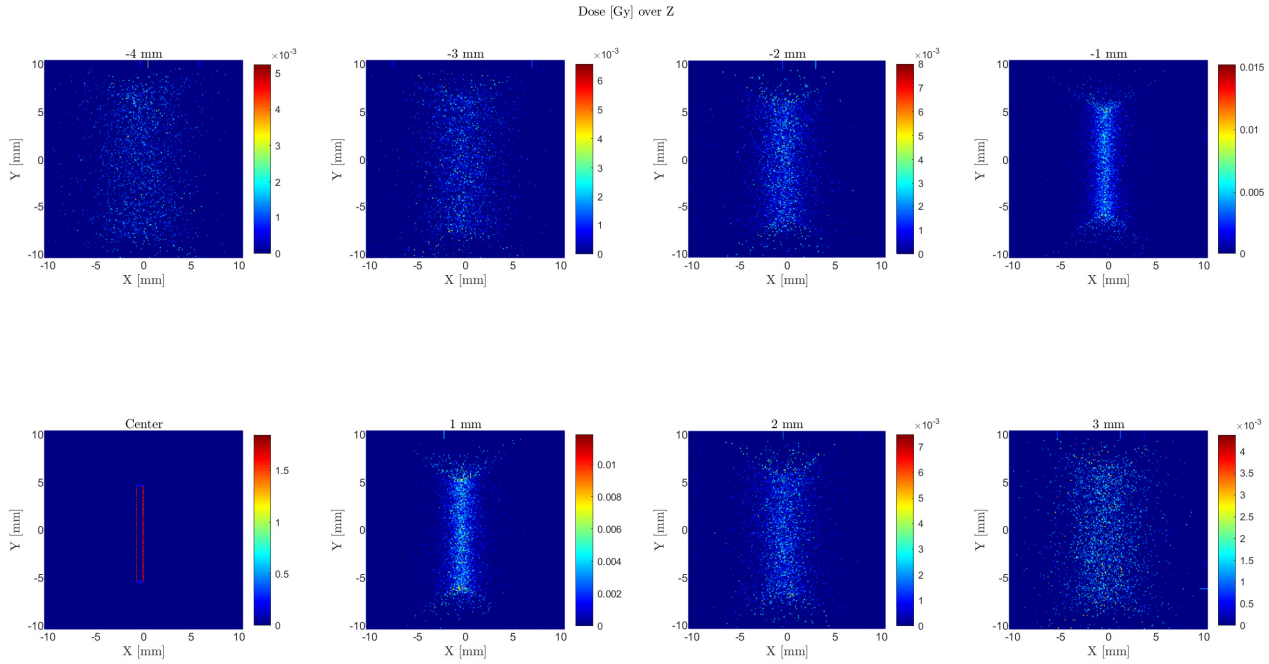

Figure 4.6: Dose distribution around the seed at different distances taken over the z-axis of the simulated world going from - 4 mm up to 3 mm away from the center of the seed (represented as the red square).

4.4 Discussion

In the past few years, the interest in using α-emitting sources to treat solid tumors in radiotherapy has increased [31–35, 89]. Maucksch, U. *et al.* (2018) [89] demonstrated the superiority of α-particles over another type of radiation by comparing the radiotoxicity produced by low- and high-LET radiation on cancerous cells under hypoxic conditions. The squamous cell carcinoma cell line A431 was irradiated using the $99m$Tc, the α-emitter ^{223}Ra, and the β-emitting ^{188}Re source. The authors demonstrated that the survival rate of the A431 cell line was significantly higher for ^{99m}Tc and ^{188}Re compared to ^{223}Ra and concluded that the optimal treatment option for hypoxic cells is through the use of α-particles.

A new promising therapeutic technique to treat solid tumors was introduced with DaRT due to the diffusion of the radioactive daughters from the decay chain of ^{224}Ra. Nonetheless, the limitation with DaRT is that the outcome will not be the same for all the patients as the diffusion length at which the diffusive daughters produced in the ^{224}Ra radioactive decay such as the ^{220}Rn and ^{212}Pb varies depending on the type of the treated tumor. Several authors have studied the response of different cancer types to DaRT through in-vitro, in-vivo studies

as well as clinical trials [16, 17, 22, 24–27, 80, 81, 90]. Overall, it has been reported that the use of DaRT leads to a favorable outcome. Cooks *et al.* (2008) [26] experimented on mice inoculated with squamous cell carcinoma. The mice developed tumors and were classified according to the tumor sizes: 3-4 mm and 6-7 mm ∅. These tumors were treated using one and two ^{224}Ra seeds. Their results showed that the DaRT treatment decreased tumor development and prolonged the mice's life expectancy. When using one DaRT seed, the tumors exhibited a significant reduction in their growth rate in both cohorts. The reduction in growth was more prominent in the less substantial tumors, leading to a necrotic region that accounted for 14% to 59% of the tumors' complete surface area. The use of two DaRT seeds was more promising since tumor eradication in 10 of the 14 animals was achieved. This suggests that the spread of ^{220}Rn and ^{212}Pb called the diffusion length, contributed to the tumor eradication and demonstrates that this diffusion length is highly dependent on the medium in which the DaRT seed is implanted. Cooks *et al.* (2009) [90] further investigated the antitumoral effects of the DaRT seeds in solid lung carcinoma (LL2, and A427). This time, the authors reported a tumor growth inhibition of 49% for the LL2 tumors and 93% for the A247.

Popovtzer, A. *et al.* (2020) performed clinical studies on 28 patients suffering from squamous cancers of the skin and head, and neck. The majority of the patients were previously treated with surgery or prior chemotherapy/radiotherapy. Complete response was reported for 78.6% of the cases while the remaining 21.4% showed a partial response to the treatment. The authors conclude that more studies should be carried out for a patient cohort with more homogeneous conditions and a better evaluation of the toxicity generated by ^{208}Pb. Popovtzer, A. *et al.* (2020) further discuss that due to the diffusion of the ^{220}Rn and ^{212}Pb, proper placement of the DaRT seeds inside the tumor will help to obtain a better and more localized dose distribution. The previous statement indicates that the number and positioning of DaRT seeds inside the tumor cannot be standardized as it will be different for each patient.

Currently, there is a lack of an α-based dosimetry software that can simulate the environmental diffusion of the daughters produced in the ^{224}Ra radioactive decay as well as the absorbed dose from all the decay products in the surrounding medium. Hence, in this study, we have developed an MC-based user code that can be used to investigate DaRT dosimetry. This user code may aid in the development of radiation detectors for acceptance testing of the applicators, quality assurance, and *in-vivo* dosimetry. The user-code

simulates the entire decay of the ^{224}Ra, transports and tracks the interactions of the emitted radiation with matter, as well as environmental diffusion of ^{220}Rn and ^{212}Pb according to the implemented *'positioning method'*.

In order to validate the user code and the implemented method, the results were compared to the reported database from the IAEA and published work [56, 88]. The obtained energy spectra from the simulation were in good agreement with the reported data from the IAEA livechart. The α-values from the energy spectrum shown in figure 4.4a were in good agreement with the database within 0.006-0.015% difference. Comparison of the continuous β-energy spectra of the results obtained in the study and the IAEA database shown in figures 4.4b, 4.4c, 4.4d shows that our results agree well with the measured data having a percentage difference of 4.812%, 0.179%, and 0.240%, respectively. Regarding the γ-energy spectrum, three relative high-intensity peaks located at 0.238, 0.583, and 2.61 MeV correspond to the metastable states of the daughters having a 0-0.081% difference with reported data.

The visualization of the *'positioning method'* was presented in figure 4.5. The tracks of the α-particles (red lines) emitted from ^{224}Ra and ^{220}Rn atoms were straight and short in length due to their high-LET resulting in a linear ionization track [2]. This means that the implemented *'positioning method'* did not affect any other particles generated during the simulation as only the positions of ^{220}Rn and ^{212}Pb atoms were modified. Implementing the numerical solution of the diffusion equation of the diffusive atoms (equations 4.3 and 4.4) directly in the Geant4 user code is challenging due to the time dependence of the equation. The preliminary *'positioning method'* implemented in this study is useful to understand the logistics of how to distribute the ^{220}Rn and ^{212}Pb atoms up to new positions depending on the numerical solution of the diffusion equations [28].

Figure 4.6 shows the resulting dose distribution from the ^{224}Ra decay and the diffusion of its α-emitter daughters at different distances from the center of the DaRT seed. As observed, α-particles are less penetrating, but thanks to the diffusion, they will deposit their energy up to $\sim 3-4$ mm from the outer diameter of the seed, creating the most biological damage as a result of their high LET. Considering the dose map located at z = 0 mm (center plane of the seed), two high-dose red lines located at $\pm$ 0.35 mm are shown. These lines correspond to the absorbed dose of the α-particles emitted from ^{224}Ra located on the surface of the seed. It was also expected to see these high-dose values at $\sim$ 2 mm around the seed. Although this is not shown in the dose map, there are dose values around the seed which seem to

be lost due to the color scale. Still, the contribution of the diffused α-particles could be observed on the other dose maps located at different distances from the center of the seed. The absorbed dose values decrease with distance in both directions (-z and +z), indicating that the α-particles can reach a distance between 3 and 4 mm from the seed. This behavior is also observed in Heger, G. *et al.* (2022) [88] work. In their work, the dose distribution of α-particles around the seed reaches a distance of $\sim$ 5 mm. Dose profiles taken over the radial distance show a decrease in dose with increasing distance. The results obtained in this thesis compared to those from Heger, G. *et al.* (2022), was similar in terms of the radial distance at which α-particles can deposit their energy.

4.5 Conclusion

In this work, a Geant4-based user code was developed to perform MC simulations of the ^{224}Ra radioactive decay, obtain its emitted energy spectra and distribute the diffusive daughters around the seed using an in-house method called the *positioning method* to obtain the absorbed dose maps from different daughters generated in the ^{224}Ra radioactive decay. The *'positioning method'* was implemented to overcome the limitation of Geant4 for not simulating the diffusion of ^{220}Rn and ^{212}Pb atoms from the DaRT seed. The energy spectra of the DaRT seed obtained with this user code were in good agreement with the values reported in the literature.

4.6 References

1. J. Pe'er, Ruthenium-106 brachytherapy, Current concepts in uveal melanoma **49**, 27–40 (2012).
2. J. DeCunha, C. Janicki, and S. Enger, A retrospective analysis of catheter-based sources in intravascular brachytherapy, Brachytherapy **16**, 586–596 (2017).
3. J. M. DeCunha and S. A. Enger, A new delivery system to resolve dosimetric issues in intravascular brachytherapy, Brachytherapy **17**, 634–643 (2018).
4. J.-J. Mazeron and A. Gerbaulet, The centenary of discovery of radium, Radiotherapy and oncology **49**, 205–216 (1998).
5. B. J. Nelson, J. D. Andersson, and F. Wuest, Targeted alpha therapy: progress in

radionuclide production, radiochemistry, and applications, Pharmaceutics **13**, 49 (2020).

6. Wikipedia, Brachytherapy.
7. L. Arazi, T. Cooks, M. Schmidt, Y. Keisari, and I. Kelson, Treatment of solid tumors by interstitial release of recoiling short-lived alpha emitters, **52**, 5025 – 5042 (2007).
8. L. Arazi, T. Cooks, M. Schmidt, Y. Keisari, and I. Kelson, The treatment of solid tumors by alpha emitters released from 224Ra-loaded sources—internal dosimetry analysis, Physics in Medicine & Biology **55**, 1203 (2010).
9. L. Arazi, Diffusing alpha-emitters radiation therapy: approximate modeling of the macroscopic alpha particle dose of a point source, Physics in Medicine & Biology **65**, 015015 (2020).
10. B. H. L. E. S. M. A. L. E. M. K. I. K. Y. Horev-Drori G, Cooks T, Local control of experimental malignant pancreatic tumors by treatment with a combination of chemotherapy and intratumoral 224radium-loaded wires releasing alpha-emitting atoms, Translational Research **159**, 32–41 (2012).
11. E. M. C. T. S. M. K. Y. K. I. Lazarov E, Arazi L, Comparative in vitro microdosimetric study of murine- and human-derived cancer cells exposed to alpha particles, Radiat. Res. **177**, 280–287 (2012).
12. T. Cooks, L. Arazi, M. Schmidt, G. Marshak, I. Kelson, and Y. Keisari, Growth retardation and destruction of experimental squamous cell carcinoma by interstitial radioactive wires releasing diffusing alpha-emitting atoms, **122**, 1657 – 1664 (2008).
13. T. Cooks, M. Schmidt, H. Bittan, E. Lazarov, L. Arazi, I. Kelson, and Y. Keisari, Local control of lung derived tumors by diffusing alpha-emitting atoms released from intratumoral wires loaded with radium-224, 74, 966 – 973 (2009).
14. T. Cooks, M. Tal, S. Raab, M. Efrati, S. Reitkopf, E. Lazarov, R. Etzyoni, M. Schmidt, L. Arazi, I. Kelson, and Y. Keisari, Intratumoral Radium-224 Loaded Wires Spread Alpha-Emitters Inside Solid Human Tumors in Ahtymic Mice Achieving Tumor Control, **32**, 5315 – 5322 (2012).
15. A. Popovtzer et al., Initial safety and tumor control results from a "first-in-human" multicenter prospective trial evaluating a novel alpha-emitting radionuclide for the treatment of locally advanced recurrent squamous cell carcinomas of the skin and head and neck, International Journal of Radiation Oncology* Biology* Physics **106**, 571–578 (2020).

16. R.-B. S, C. H, S. M, C. T, E. M, A. L, R.-W. L, M. G, K. I, and K. Y., Ablation of experimental colon cancer by intratumoral 224Radium-loaded wires is mediated by alpha particles released from atoms which spread in the tumor and can be augmented by chemotherapy, Int J Radiat Biol. , 179–186 (2015).
17. H. Park, H. Paganetti, J. Schuemann, X. Jia, and C. H. Min, Monte Carlo methods for device simulations in radiation therapy, Physics in Medicine & Biology **66**, 18TR01 (2021).
18. X.-. M. C. Team, MCNP—A General N-Particle Transport Code, Version **5**, 2003.
19. I. Kawrakow, The EGSnrc code system, Monte Carlo simulation of electron and photon transport, NRCC Report Pirs-701 (2001).
20. S. Agostinelli and et al., Geant4—a simulation toolkit, Nuclear Instruments and Methods in Physics Research Section A **503**, 250–303 (2003).
21. T. B ohlen, F. Cerutti, M. Chin, A. Fass'o, A. Ferrari, P. G. Ortega, A. Mariani, P. R. Sala, G. Smirnov, and V. Vlachoudis, The FLUKA code: developments and challenges for high energy and medical applications, Nuclear data sheets **120**, 211–214 (2014).
22. F. Salvat et al., PENELOPE-2008: A code system for Monte Carlo simulation of electron and photon transport, in Workshop Proceedings, Barcelona, Spain, volume **30**, 2008.
23. IAEA, National Nuclear Data Center.
24. V. Ivantchenko, Electromagnetic Physics: Geant4 Advanced Course.
25. Geant4, Book For Application Developers.
26. E. Mendoza, D. Cano-Ott, P. Romojaro, V. Alcayne, P. G. Abia, V. Pesudo, and R. S. L. Romero, Neutron production induced by α-decay with Geant4, Nuclear Instruments and Methods in Physics Research Section A: Accelerators, Spectrometers, Detectors and Associated Equipment **960** (2020).
27. I. Sechopoulos, D. W. O. Rogers, M. Bazalova-Carter, W. E. Bolch, E. C. Heath, M. F. McNitt-Gray, J. Sempau, and J. F. Williamson, RECORDS: improved Reporting of montE CarlO RaDiation transport Studies: Report of the AAPM Research Committee Task Group 268, Med. Phys. **45** (2017).
28. D. R. A. of Canada, Digital Research Alliance of Canada.
29. J. Baro, J. Sempau, J. M. Fern andez-Varea, and F. Salvat, PENELOPE: An algorithm for Monte Carlo simulation of the penetration and energy loss of electrons and positrons in matter, Nuclear Inst. and Methods in Physics Research B, 31.

30. I. A. E. Agency, IAEA - Nuclear Data Section.
31. FLUKA, Introduction to the Monte Carlo simulation of radiation transport.
32. A. F. Bielajew, Fundamentals of the Monte Carlo method for neutral and charged particle transport, (2001).
33. G. Heger, A. Roy, M. Dumancic, and L. Arazi, Alpha dose modeling in diffusing alpha-emitters radiation therapy—Part I: single-seed calculations in one and two dimensions, Medical Physics n/a.
34. P. S. and et al., α-Emitters for Radiotherapy: From Basic Radiochemistry to Clinical Studies-Part 1, J. Nucl. Med. **6**, 878 – 884 (2018).
35. P. S. and et al., α-Emitters for Radiotherapy: From Basic Radiochemistry to Clinical Studies-Part 2, J. Nucl. Med. **7**, 1020 – 1027 (2018).
36. P. J. and C. J., Revisiting the Radiobiology of Targeted Alpha Therapy, Frontiers in Medicine **8**, 1020 – 1027 (2021).
37. T. NK and et al., Development of Targeted Alpha Particle Therapy for Solid Tumors, Molecules **24** (2019).
38. N. S and G. A, Targeted Alpha Particle Therapy for Neuroendocrine Tumours: The Next Generation of Peptide Receptor Radionuclide Therapy, Neuroendocrinology **108**, 256 – 264 (2019).
39. C. J. C. N. Larson, S., Radioimmunotherapy of human tumours, Nature Reviews Cancer **15**, 347–360 (2015).
40. S. S. D.-M. M. Couturier, O., Cancer radioimmunotherapy with alpha-emitting nuclides, European Journal of Nuclear Medicine and Molecular Imaging **32**, 601–614 (2005).
41. E. M. H. I. U. V. K. I. K. Y. Confino H, Schmidt M, Inhibition of mouse breast adenocarcinoma growth by ablation with intratumoral alpha-irradiation combined with inhibitors of immunosuppression and CpG, Cancer Immunology, Immunotherapy 65, 1149–1158 (2016).
42. J. T. Bushberg, J. A. Seibert, E. M. L. Jr., and J. M. Boone, The Essential Physics of Medical Imaging, volume 3, LIPPINCOTT WILLIAMS WILKINS, 2012.

4.7 Author contributions statement

4.8 Additional information

Competing interests The authors declare no competing interests.

Acknowledgments The authors acknowledge funding from the Canada Research Chair Program 252136), the TransMedTech Institute's activities, and thanks, in part, to funding from the Canada First Research Excellence Fund. Victor Diaz acknowledges funding from the Mexican institution Consejo Nacional de Ciencia y Tecnología (CONACyT) for granting him the CONACyT-Regional Centro 2020' scholarship to pursue a postgraduate study at McGill University, Canada. Computations were performed on the Cedar cluster of the Digital Research Alliance of Canada.

Chapter 5

Discussion

Brachytherapy, especially with MRI guidance, is one of the most effective and precise radiation delivery modalities for the treatment of certain tumor types. Compared with external beam radiotherapy, brachytherapy delivers high doses of radiation to the tumor, which rapidly falls off with distance from the source allowing it to spare the surrounding healthy tissues. In addition, brachytherapy is efficient, precise, and cost-effective. About 60% of radiation oncology clinics across Canada offer this treatment modality for gynecological, genitourinary, and lower gastrointestinal cancers as the most treated sites [91, 92]. A study by Lecavalier *et. al* (2021) showed overall steady use of brachytherapy between 2011 and 2019 in Quebec, Canada [91].

The most commonly used radioactive sources in brachytherapy emit high-energy photons which travel long distances inside the patient reaching the surrounding healthy tissue and causing toxicity. Low LET radiation, such as photons, primarily causes indirect DNA damage through the production of free radicals such as hydroxyl radicals (OH). The free radicals can diffuse some distance through the cell before interacting with the DNA, leading to sparse energy depositions and hence damage to multiple sites on the DNA molecule i.e., single-strand breaks, which are often easily repairable by the cell. On the other hand, high-LET radiation such as α-particles, is much more densely ionizing than low-LET radiation and leads to a higher probability of direct DNA damage. During direct DNA damage, the ionizing particles interact directly with the DNA molecule. The caused damage is severe and more localized, resulting in complex DNA damage, including double-strand breaks, which can be

difficult for the cell to repair.

As described above, low LET radiation primarily causes indirect DNA damage through the production of free radicals, hence leading to less DNA damage in the hypoxic regions of a tumor. For the treatment of hypoxic tumors, the use of α-particles is a more promising option due to their high LET and production of direct DNA damage, which is independent of the level of oxygen present in the cells.

Several studies have investigated the effect of different radioactive sources on cancerous cell lines under hypoxic conditions. Maucksch, U. *et al.* (2018) [89] proposed the use of Meitner-Auger electrons emitted from the decay of ^{99m}Tc (also a 140 keV photon-emitter) as a potential therapeutic option for hypoxic tumor cells treatment. The α-emitter ^{223}Ra and β-emitter ^{188}Re were tested as well for comparison. The authors irradiated squamous cell carcinoma cell line A431 with the three sources mentioned above. It was found that the survival rate of this cell line was significantly higher for ^{99m}Tc and ^{188}Re compared to ^{223}Ra. Their results indicated that the radiotoxic effects of ^{99m}Tc and ^{188}Re present a higher dependence on oxygen levels. They conclude that the use of ^{99m}Tc does not represent any therapeutic potential for treating hypoxic tumors and that the best way to treat hypoxic tumors is through the use of α-particles.

The main limitation of α-particles for treating solid tumors is their short range, however, α-emitting sources are gaining popularity in radiotherapy [31–35]. With the advent of DaRT, it is possible to treat solid tumors due to the diffusion of the radioactive daughters from the decay chain of ^{224}Ra in the tumors. However, DaRT has limitations *per se* since the outcome will not be the same for all patients because the diffusion length of the diffusive daughters varies depending on the type of the treated tumor.

Previous studies have investigated this technique using different cancer cell lines in mice and clinical studies [16,17,22,24–27,80,81,90]. Overall these studies show that DaRT can lead to tumor shrinkage. For instance, Cooks *et al.* (2008) [26] performed several experiments on mice with squamous cell carcinoma tumors of different sizes (3-4 mm and 6-7 mm ∅) using one and two ^{224}Ra seeds. Their results showed that the treatment with DaRT seeds retarded tumor development and prolonged life expectancy. The results using one DaRT seed in both groups of tumors (3-4 mm and 6-7 mm) showed a considerably retarded tumor

growth, especially in the smaller tumors which had a better treatment response, resulting in a necrotic region of 14-59% of the total area of the tumors. The use of two DaRT seeds resulted in tumor eradication in 10 of the 14 animals. Their results were more promising when using two DaRT seeds and suggest that this may be because the spread of the radioactive daughters in the tumor was due to blood flow. This demonstrates once again that the diffusion of the daughters is highly dependent on the medium in which they are immersed. The vascularization or no-vascularization of the tumor will allow the spread of ^{212}Pb. In another study [90], this group investigated the response of tumors (6-7 mm) using the Lewis lung carcinoma (LL2) and the human-derived A427 cancer cell lines with a single seed. The results once again showed significant tumor growth inhibition of 49% for LL2 tumors and 93% for A247. Analysis of the distribution of diffusive daughters was carried out by autoradiography. Cooks *et al.* (2009) [27] conclude that the combination of two DaRT seeds with therapeutic drugs represents a great potential in alpha-based radiotherapy.

The clinical study conducted by Popovtzer, A. *et al.* (2019) [80] focused on studying the feasibility and safety of using DaRT for the treatment of squamous cancers of the skin, head, and neck. The cohort of patients chosen had an unfavorable prognosis and most of the patients were previously treated with surgery or prior chemotherapy/radiotherapy. In this study, 31 lesions were studied in 28 patients, 78.6% of these lesions showed a complete response to DaRT treatment, while the remaining 21.4% showed a partial response to the treatment. Although the clinical studies showed great promising results, the authors conclude that more studies should be carried out to include a patient cohort with more homogeneous conditions and a better evaluation of the toxicity generated by ^{208}Pb. Popovtzer, A. *et al.* (2019) further discuss that due to the 5 mm dose cloud from the seed generated by the diffusion of the ^{220}Rn daughter, a proper seed placement within the tumor will help to obtain a better dose distribution by limiting the exposure of healthy tissue. This indicates that the number and positioning of DaRT seeds inside the tumor cannot be standardized as it will be different depending on the tumor characteristics for each patient. This reveals the importance of developing a robust α-based dosimetric protocol. Within this field, the applications of DaRT are in film dosimetry, autoradiography, and the development of detectors to ensure a quality assurance (QA) protocol for DaRT applicators prior to seed insertion into the

patient, as well as the development of *in-vivo* detectors. Detector development or dosimetry investigations for this novel brachytherapy source require the development of MC-based dosimetry software.

To obtain accurate results from the MC simulations, it is important to model the DaRT source, all the physical decay processes as well as the environmental diffusion of the ^{224}Ra radioactive daughters, which requires considering the patient-specific tumor structure. To account for environmental diffusion in patient-specific tumor geometry in MC simulations is currently not possible, however, Arazi et al. (2020) [28] proposed an approximate diffusion model as a starting point in which the tumor is assumed to be a homogeneous, isotropic and a time-independent medium. In this thesis, the α-based dosimetry was addressed by means of an in-house developed MC-based user-code for film dosimetry and to study the dose distribution around the DaRT seeds. The developed in-house software will be used for DaRT dosimetry and the development of detectors for DaRT.

For film dosimetry applications, the response of the unlaminated GafChromic® EBT3 film to alpha radiation was studied by means of MC simulations to calculate the dose rate used for film calibration under specific conditions. The use of the unlaminated GafChromic® EBT3 film is more affordable for DaRT dosimetry than modern high-resolution autoradiography setups. The latter ones are currently used to investigate the diffusion length of the ^{224}Ra radioactive daughters: ^{220}Rn and ^{212}Pb. The calculated dose rate was used to define film irradiation times and to obtain a calibration curve for the analysis of the irradiated films. The user code developed with the Geant4 simulation toolkit allows a detailed simulation of the geometry and decay of a radioactive source. The radioactive sources simulated in this thesis were an ^{241}Am source and the DaRT seed with ^{224}Ra. To validate the developed user code, the obtained results were compared with reported database values and published work. The results from film simulation include the emitted energy spectra and the calculated dose rate. The main peak values of the ^{241}Am decay energy spectrum were compared to those values from the database published by NIST and IAEA [56, 57]. The comparison for each value was found to be in good agreement since there was a 0.036-0.516% range difference. In addition to this, the shape of the energy spectrum is the same as the ones measured in published work by Demir. *et al.* (2013) [68] and Ramirez-Jimenez, F. J. (2006) [69]. The

comparison between the database and published work indicates that the simulation of the active source is accurate. As for the dose rate, it was compared with the results obtained by Ramos-Moreira (2020) [44]. In his work, he also studied the response of EBT3 model GafChromic® films to α-radiation. In this thesis, the dose rate for the LiPCDA (water-like material) active layer was 1.09 ± 0.04 Gy/min within a region of interest of 1 mm ⌀. On the other hand, the value reported by Ramos-Moreira (2020) was $\sim$ 2.4 Gy/min. Despite our results were in the same order of magnitude, the difference between the dose rate values was due to the use of a different simulation toolkit and the simulation input parameters. The input parameters were summarized in table 3.4.

The simulation toolkit used by Ramos-Moreira (2020) was TOPAS (a wrapper on top of Geant4) which has some limitations compared to Geant4. When comparing TOPAS and Geant4 in terms of this thesis, TOPAS has a limitation, which is not having ^{241}Am defined in its material library. Hence, the active source volume material defined in his study was defined as hafnium (Hf). Instead of simulating the radioactive decay of ^{241}Am, α-particles were randomly generated in the Hf volume with a mean emission energy of 5.48 MeV. The difference in the atomic number of Hf (72) and ^{241}Am (95) will have an impact on the scored absorbed dose. ^{241}Am as an active volume material will result in a lower number of α-particles reaching the scoring volumes, contributing to less dose. The active source volume and regions of interest used by Ramos-Moreira (2020) were larger compared to the ones defined in this thesis: 5×5 cm^2 compared to 5 mm ⌀ for the active source volume, and 3.4 cm ⌀ compared to 1 mm ⌀ for the region of interest. The difference in the actual activities of the sources was yet another important factor for the simulations. The actual activity of the source was used for the normalization of the results. The source activity used in Ramos-Moreira's (2020) work was 7.4 MBq, which is orders of magnitude greater than the activity of the source used in this thesis, 30.05 kBq. In both studies, the normalization of the dose rate was performed according to equation 5.1, from which it can be seen the dependency between the dose rate and the activity of the source.

$$\dot{D} = \frac{D_{sim} \times Act_{source}}{N_{emitted}} \left[\frac{Gy}{s}\right], \tag{5.1}$$

In the normalized dose rate equation, D_{sim} is the simulated scored dose in the scoring voxels, Act_{source} is the activity of the source, and $N_{emitted}$ is the number of *emitted* particles (generated runs). All these

The results presented in this work can be considered to be reliable since the geometry, composition of the source, and film were simulated and modeled in detail. The dose rate value in water was obtained to have an estimate of the absorbed dose in tissue for clinical purposes. The implemented user code can be applied to other configurations of α-particle emitting sources, radiochromic films, and surrounding media.

DaRT dosimetry is challenging [28] and the development of dosimetry tools such as quality assurance and *in-vivo* detectors is challenging since these dosimeters will be required to respond to α, β, and γ radiation. In terms of *in-vivo* dosimetry, an accurate representation of the diffusion behavior of the radioactive daughters of ^{224}Ra must be taken into account in the MC simulations. Nevertheless, the diffusion of ^{220}Rn and ^{212}Pb are not simulated by the Geant4 simulation toolkit. Therefore, the implementation of the solution of the diffusion equations of the diffusive atoms should be included in the MC-based user code. This implementation directly in the Geant4 user code is challenging due to the time dependence of the equation.

The general model derived by Arazi *et al.* (2020) describing the diffusion of ^{220}Rn and ^{212}Pb is complex due to several factors involved in their complete solutions. One of the factors includes time-dependent information in the sub-millimeter scale that are clinically unavailable [28]. Moreover, the transportation of the diffusive daughters inside the tumor highly depends on the tumor microenvironment. The tumor microenvironment is complex, can vary between tumor regions, and can change through time. Instead, Arazi *et al.* (2020) derived a simplified model assuming that the medium is homogeneous, isotropic, and time-independent. For this work, this simplified model of the diffusion equations was considered. The diffusive daughters were distributed around the DaRT seed with an implemented method called the *'positioning method'*.

To validate the user code and the implemented method, the results were compared to the reported database from the IAEA and published work. The obtained energy spectra from the simulation were found to be in good agreement with the ones reported by the

IAEA livechart. The simulated α-particle energy spectrum compared to the database, had an acceptable percentage difference of 0.006-0.015%. As for the continuous β-particle energy spectra of ^{212}Pb, ^{212}Bi, and ^{208}Tl, they had a percentage difference of 4.812%, 0.179%, and 0.240%, respectively in comparison to measured data. Regarding the γ-energy spectrum, it exhibits three relative high-intensity peaks, each of 0.238, 0.583, and 2.61 MeV, respectively. These three γ energies correspond to the metastable states of the daughters, and had a percentage difference up to 0.081% with the database. Due to the relatively high intensity of the three γ photons, especially the 2.62 MeV, they can be used in the calibration of QA detector systems for DaRT.

The *'positioning method'* was assessed using a visualization of the simulation and through dose maps taken at different positions from the center of the seed. The visualization of this method (figure 4.5) shows the α-particles tracks (red lines) emitted from ^{224}Ra and ^{220}Rn atoms. These tracks were straight and short in length since α-particles are high-LET radiation, resulting in a linear ionization track [2]. This means that the implemented *'positioning method'* did not affect any other radioactive daughters of ^{224}Ra or any emitted radiation. Only the positions of ^{220}Rn and ^{212}Pb atoms were modified. The *'positioning method'* implemented in this thesis is useful to understand the logistics of how to distribute the ^{220}Rn and ^{212}Pb atoms up to new positions depending on the solution of the diffusion equations [28]. The dose maps presented in figure 4.6 showed the resulting dose distribution from the ^{224}Ra decay and the diffusion of its α-emitter daughters. These dose maps show that the diffusion of ^{220}Rn and ^{212}Pb allows α-particles to deposit their energy up to $\sim 3-4$ mm from the outer diameter of the seed. Despite this fact, more particles should be run to obtain a reliable dose value and reduce the uncertainty so that these results can be compared to Heger, G. *et al.* (2022) [88] work.

Future work will include simulating more particles to compare this last simulation with published work and adapting this user code to the GEANT4-DNA simulation toolkit to simulate a more realistic cell-like environment. Regardless of the need for higher statistics, the results presented in this work show that the *positioning method* using the solution of the diffusion equations, is a feasible method to simulate the diffusion of the diffusive daughters in DaRT.

This Geant4-based user code will be used to benchmark the animal studies that will be performed in our institution to study the diffusion length of ^{220}Rn and ^{212}Pb for different types of cancers. Such studies will include autoradiography measurements as well as film measurements using the unlaminated GafChromic® EBT3 film. Therefore the implemented *'position method'* can be used in conjunction with the film geometry and composition to compare the experimental results. This will aid in the development of a more robust α-based dosimetry protocol that includes different types of tumors and detectors.

Chapter 6

Conclusion and Future Work

In this thesis, an in-house Monte Carlo dosimetry package for α particle dosimetry was developed. MC simulations with this software were performed to study the response of the unlaminated GafChromic® EBT3 film to α radiation and to study the dose distribution of α-particles around the DaRT seed.

The simulated ^{241}Am decay energy spectra for the unlaminated GafChromic® EBT3 film study were in good agreement with published work. The calculated dose rate for the film was of the same order of magnitude. The variation was due to differences in simulated geometry and input parameters.

This user code can be applied to other configurations of α-particle emitting sources, for dosimetry and detector development purposes. Such α-emitting sources may be the DaRT seeds. Therefore this user code was further improved by implementing the *'positioning method'* to distribute the diffusive daughters of ^{224}Ra.

This improvement allowed us not only to obtain the emitted energy spectra from the DaRT seed but also to diffuse the diffusive daughters around the seed according to their respective diffusion equations. These results were useful to have a clearer idea of what type of dose distribution is expected from the seeds.

Further research will consist of constructing Dart QA and *in-vivo* detectors, testing and benchmarking them with this developed user code. The code will be complemented with animal studies so that it can be used as an α-dosimetry package for film, QA, and *in-vivo* dosimetry.

Bibliography

[1] C. C. Society, "Cancer statistics at a glance."

[2] E. M. L. J. J. M. B. Jerrold T. Bushberg, J. Anthony Seibert, *The Essential Physics of Medical Imaging*, vol. 3. LIPPINCOTT WILLIAMS WILKINS, 2012.

[3] E. B. Podgorsak, *Radiation Physics for Medical Physicists*, vol. 3. Springer, 2016.

[4] M. E. P. Simon R. Cherry, James A. Sorenson, *Physics in Nuclear Medicine*, vol. 4. SAUNDERS ELVESIER, 2012.

[5] K. J., *Notes taken from the MDPH 613 Health Physics*. Medical Physics Unit, McGill University, Canada, 2020.

[6] T. A. C. S. medical and editorial content team, "Getting internal radiation therapy (brachytherapy)."

[7] J. Pe'er, "Ruthenium-106 brachytherapy," *Current concepts in uveal melanoma*, vol. 49, pp. 27–40, 2012.

[8] J. DeCunha, C. Janicki, and S. Enger, "A retrospective analysis of catheter-based sources in intravascular brachytherapy," *Brachytherapy*, vol. 16, no. 3, pp. 586–596, 2017.

[9] J. M. DeCunha and S. A. Enger, "A new delivery system to resolve dosimetric issues in intravascular brachytherapy," *Brachytherapy*, vol. 17, no. 3, pp. 634–643, 2018.

[10] Wikipedia, "Brachytherapy."

[11] Y. N., *Notes taken from the MDPH 609 Radiation Biology course*. Medical Physics Unit, McGill University, Canada, 2021.

[12] Wikipedia, "Oxygen effect."

[13] E. Alizadeh, A. G. Sanz, G. Garcia, and L. Sanche, "Radiation damage to dna: The indirect effect of low-energy electrons," *The journal of physical chemistry letters*, vol. 4, no. 5, pp. 820–825, 2013.

[14] U. Maucksch, R. Runge, L. Oehme, J. Kotzerke, and R. Freudenberg, "Radiotoxicity of alpha particles versus high and low energy electrons in hypoxic cancer cells," *Nuklearmedizin-NuclearMedicine*, vol. 57, no. 02, pp. 56–63, 2018.

[15] D. Ganten and K. Ruckpaul, *Encyclopedic reference of genomics and proteomics in molecular medicine*. Springer, 2006.

[16] S. M. K. Y. K. I. Arazi L, Cooks T, "Treatment of solid tumors by interstitial release of recoiling short-lived alpha emitters," *Phys. Med. Biol.*, vol. 52, pp. 5025–5042, 2007.

[17] S. M. K. Y. K. I. Arazi L, Cooks T, "The treatment of solid tumors by alpha emitters released from (224)Ra-loaded sources-internal dosimetry analysis," *Phys. Med. Biol.*, vol. 55, pp. 1203–1218, 2010.

[18] C. J. C. N. Larson, S., "Radioimmunotherapy of human tumours," *Nature Reviews Cancer*, vol. 15, pp. 347–360, 2015.

[19] S. S. D.-M. M. Couturier, O., "Cancer radioimmunotherapy with alpha-emitting nuclides," *European Journal of Nuclear Medicine and Molecular Imaging*, vol. 32, pp. 601–614, 2005.

[20] M. L. B. G. G. A. W. V. U. M. S.-H. N. B. C. K. A. C. J. S. C. U. M. B. P. T. A. I. H. Zacherl MJ, Gildehaus FJ, "First Clinical Results for PSMA-Targeted α-Therapy Using 225Ac-PSMA-IT in Advanced-mCRPC Patients," *J. Nuc. Med.*, vol. 62, pp. 669 – 674, 2021.

[21] AlphaTau, "Alpha dart^{TM} technology."

[22] B. H. L. E. S. M. A. L. E. M.-K. I. K. Y. Horev-Drori G, Cooks T, "Local control of experimental malignant pancreatic tumors by treatment with a combination

of chemotherapy and intratumoral 224radium-loaded wires releasing alpha-emitting atoms," *Translational Research*, vol. 159, pp. 32–41, 2012.

[23] E. M. C. T. S. M. K. Y. K. I. Lazarov E, Arazi L, "Comparative in vitro microdosimetric study of murine- and human-derived cancer cells exposed to alpha particles," *Radiat. Res.*, vol. 177, pp. 280–287, 2012.

[24] E. M. H. I. U. V. K. I. K. Y. Confino H, Schmidt M, "Inhibition of mouse breast adenocarcinoma growth by ablation with intratumoral alpha-irradiation combined with inhibitors of immunosuppression and CpG," *Cancer Immunology, Immunotherapy*, vol. 65, pp. 1149–1158, 2016.

[25] R. S. E. M. R. S. L. E. E. R. S. M. A. L. K. I. K. Y. Cooks T, Tal M, "Intratumoral 224Ra-loaded wires spread alpha-emitters inside solid human tumors in athymic mice achieving tumor control," *Anticancer Research*, vol. 32, pp. 5315–5322, 2012.

[26] T. Cooks, L. Arazi, M. Schmidt, G. Marshak, I. Kelson, and Y. Keisari, "Growth retardation and destruction of experimental squamous cell carcinoma by interstitial radioactive wires releasing diffusing alpha-emitting atoms," *International journal of cancer*, vol. 122, no. 7, pp. 1657–1664, 2008.

[27] T. Cooks, L. Arazi, M. Efrati, M. Schmidt, G. Marshak, I. Kelson, and Y. Keisari, "Interstitial wires releasing diffusing alpha emitters combined with chemotherapy improved local tumor control and survival in squamous cell carcinoma-bearing mice," *Cancer*, vol. 115, no. 8, pp. 1791–1801, 2009.

[28] A. L, "Diffusing alpha-emitters radiation therapy: approximate modeling of the macroscopic alpha particle dose of a point source," *Phys. Med. Biol.*, vol. 65, 2020.

[29] A. F. H., *Introduction to Radiological Physics and Radiation Dosimetry*. Wiley-VCH Verlag GmbH Co. KGaA, 1986.

[30] C. B. Saw, A. S. Meigooni, and R. Nath, "Review of aapm task group no. 43 recommendations on interstitial brachytherapy sources dosimetry," *Medical dosimetry*, vol. 23, no. 4, pp. 259–263, 1998.

[31] P. S. and et al., "α-Emitters for Radiotherapy: From Basic Radiochemistry to Clinical Studies-Part 1," *J. Nuc. Med.*, vol. 6, pp. 878 – 884, 2018.

[32] P. S. and et al., "α-Emitters for Radiotherapy: From Basic Radiochemistry to Clinical Studies-Part 2," *J. Nuc. Med.*, vol. 7, pp. 1020 – 1027, 2018.

[33] P. J. and C. J., "Revisiting the Radiobiology of Targeted Alpha Therapy," vol. 8, pp. 1020 – 1027, 2021.

[34] T. NK and et al., "Development of Targeted Alpha Particle Therapy for Solid Tumors," vol. 24, 2019.

[35] N. S and G. A, "Targeted Alpha Particle Therapy for Neuroendocrine Tumours: The Next Generation of Peptide Receptor Radionuclide Therapy," vol. 108, pp. 256 – 264, 2019.

[36] W. McLaughlin and L. Chalkley, "Measurement of Radiation Dose Distributions with Photochromic," *Radiology*, vol. 84, pp. 124 – 125, 1965.

[37] S. Devic, J. Seuntjeans, E. Sham, and E. B. Podgorsak, "Precise Radiochromic Film Dosimetry Using a Flat-bed Document Scanner," *Med. Phys.*, vol. 32, pp. 2245 – 2253, 2005.

[38] S. Devic, "Radiochromic Film Dosimetry: Past, present, and future," *Euro. J. Med. Phys*, vol. 27, pp. 122 – 134, 2011.

[39] S. Devic, N. Tomic, and D. Lewis, "Reference Radiochromic Film Dosimetry: Review of Technical Aspects," *Euro. J. Med. Phys*, vol. 32, pp. 541 – 556, 2016.

[40] S. Aldelaijan and S. Devic, "Comparison of Dose Response Functions for EBT3 model Gafchromic Film Dosimetry," *Euro. J. Med. Phys*, vol. 49, pp. 112 – 118, 2018.

[41] A. S. Mustaquim, S. Kandaiya, N. N. A. Razak, and N. Z. Yahaya, "The Gafchromic EBT3 film as alpha detector," *J. Phys.: Conf. Ser.*, vol. 1083, pp. 12 – 19, 2018.

[42] K. Y. C.Y.P. Ng, S.L. Chun, "Quality assurance of alpha-particle dosimetry using peeled-off Gafchromic EBT3® film," *Radiation Physics and Chemistry*, vol. 125, pp. 176–179, 2016.

[43] B. U. H. R. K. J. Mukherjee B, Gholami YH, "A unique alpha dosimetry technique using Gafchromic EBT3® film and feasibility study for an activity calibrator for alpha-emitting radiopharmaceuticals ," *Brit. J. Radiol.*, vol. 88, 2015.

[44] H. M. R. Moreira, "Investigating the mechanisms of α-particle therapy in prostate cancer," 2020.

[45] K.-H. Lee, J.-Y. Shin, and E.-H. Kim, "Measurement of activity distribution in an Am-241 disc source using peeled-off Gafchromic EBT3 films," *Appl. Radiat. Isotopes*, vol. 135, pp. 192 – 200, 2018.

[46] S. Agostinelli and et al., "Geant4—a simulation toolkitt," *Nuclear Instruments and Methods in Physics Research Section A*, vol. 503, pp. 250–303, 2003.

[47] G. Famulari, "Dynamic-shield intensity modulated brachytherapy for prostate cancer," 2020.

[48] S. Incerti, "A practical introduction to the Geant4 Monte Carlo simulation toolkit," *Nuclear Instruments and Methods in Physics Research Section A*.

[49] S. J and et al., "Evaluation of Gafchromic® EBT3 films characteristics in therapy photon, electron and proton beams," *Physica Medica*, vol. 29, pp. 599 – 606, 2013.

[50] R. Dreindl, D. Georg, and M. Stock, "Radiochromic film dosimetry: Considerations on precision and accuracy for EBT2 and EBT3 type films," *Zeitschrift für Medizinische Physik*, vol. 24, pp. 153–163, 2014.

[51] K. S and et al., "Characteristic of EBT-XD and EBT3 radiochromic film dosimetry for photon and proton beams," *Phys. Med. Biol.*, vol. 63, 2018.

[52] M. Martisikova, B. Ackermann, and O. Jackel, "Analysis of Uncertainties in Gafchromic EBT Film Dosimetry of Photon Beams," *Phys. Med. Biol.*, vol. 53, pp. 7013 – 7027, 2008.

[53] A. G. D. Films, "Gafchromic ebt."

[54] C. R and et al., "Dose-response of EBT3 radiochromic films to proton and carbon ion clinical beams," *Phys. Med. Biol.*, vol. 62, 2017.

[55] A. I. Kassis, "Therapeutic Radionuclides: Biophysical and Radiobiologic Principles," vol. 38, pp. 358 – 366, 2008.

[56] I. A. E. Agency, "Iaea - nuclear data section."

[57] N. I. of Standards and Technology, "X-ray transition energy database."

[58] V. Ivantchenko, "Electromagnetic physics: Geant4 advanced course."

[59] Geant4, "Book for application developers."

[60] E. Mendoza, D. Cano-Ott, P. Romojaro, V. Alcayne, P. G. Abia, V. Pesudo, and R. S. L. Romero, "Neutron production induced by α-decay with Geant4," *Nuclear Instruments and Methods in Physics Research Section A: Accelerators, Spectrometers, Detectors and Associated Equipment*, vol. 960, 2020.

[61] I. Sechopoulos, D. W. O. Rogers, M. Bazalova-Carter, W. E. Bolch, E. C. Heath, M. F. McNitt-Gray, J. Sempau, and J. F. Williamson, "RECORDS: improved Reporting of montE CarlO RaDiation transport Studies: Report of the AAPM Research Committee Task Group 268," *Med. Phys.*, vol. 45, 2017.

[62] D. R. A. of Canada, "Digital research alliance of canada."

[63] J. Baró, J. Sempau, J. M. Fern´andez-Varea, and F. Salvat, "PENELOPE: An algorithm for Monte Carlo simulation of the penetration and energy loss of electrons and positrons in matter," vol. 100, pp. 31–46, 1995.

[64] FLUKA, "Introduction to the monte carlo simulation of radiation transport."

[65] A. F. Bielajew, "Fundamentals of the monte carlo method for neutral and charged particle transport," *The University of Michigan*, vol. 1, 2001.

[66] S. Devic, J. Seuntjens, G. Hegyi, E. Podgorsak, C. Soares, A. Kirov, I. Ali, J. Williamson, and A. Elizondo, "Dosimetric properties of improved GafChromic films for different digitizers," *Med. Phys.*, vol. 31, pp. 2392 – 2401, 2004.

[67] G. F. Knoll, *Radiation Detection and Measurement*. John Wiley Sons, Inc., 2000.

[68] D. Demir, M. Eroglu, and A. Tursucu, "Studying of characteristics of the HPGe detector for radioactivity measurements," vol. 8, 2013.

[69] *X-ray Spectroscopy with PIN diodes*, vol. 857.

[70] J. Perl *et al.*, "Topas: an innovative proton monte carlo platform for research and clinical applications," *Medical physics*, vol. 39, no. 11, pp. 6818–6837, 2012.

[71] L. KM, L. US, and K. EH, "A practical alpha particle irradiator for studying internal alpha particle exposure," *Appl. Radiat. Isotopes*, vol. 115, pp. 304 – 311, 2016.

[72] H. El-Naggar, E. Ghanim, M. E. Ghazaly, and T. Salama, "On the reigstration of low energy alpha particle with modified GafChromic EBT2 radiochromic film," vol. 191, pp. 1 – 6, 2022.

[73] S. Devic, "Radiochromic Film Dosimetry: Past, present and future," *Euro. J. Med. Phys*, vol. 27, pp. 122 – 134, 2011.

[74] D. Kirby *et al.*, "LET dependence of GafChromic films and an ion chamber in low-energy proton dosimetry," *Phys. Med. Biol.*, vol. 55, pp. 417 – 433, 2010.

[75] S. Vallières *et al.*, "Low-energy proton calibration and energy-dependence linearization of ebt-xd radiochromic films," *Review of Scientific Instruments*, vol. 90, no. 8, p. 083301, 2019.

[76] J. B. Marion and M. L. Roush, *The Effects of Nuclear Radiations*, vol. 2. Academic Press, Inc., 1974.

[77] A. Aydarous and M. E. Ghazaly, "Characterization of HD-V2 Gafchromic Film for Measurement of Spatial Dose Distribution from Alpha Particle of 5.5 MeV," vol. 7, pp. 1174 – 1176, 2013.

[78] J.-J. Mazeron and A. Gerbaulet, "The centenary of discovery of radium," *Radiotherapy and oncology*, vol. 49, no. 3, pp. 205–216, 1998.

[79] B. J. Nelson, J. D. Andersson, and F. Wuest, "Targeted alpha therapy: progress in radionuclide production, radiochemistry, and applications," *Pharmaceutics*, vol. 13, no. 1, p. 49, 2020.

[80] A. Popovtzer, E. Rosenfeld, A. Mizrachi, S. Bellia, R. Ben-Hur, G. Feliciani, A. Sarnelli, L. Arazi, L. Deutsch, I. Kelson, *et al.*, "Initial safety and tumor control results from a "first-in-human" multicenter prospective trial evaluating a novel alpha-emitting radionuclide for the treatment of locally advanced recurrent squamous cell carcinomas of the skin and head and neck," *International Journal of Radiation Oncology* Biology* Physics*, vol. 106, no. 3, pp. 571–578, 2020.

[81] R.-B. S, C. H, S. M, C. T, E. M, A. L, R.-W. L, M. G, K. I, and K. Y., "Ablation of experimental colon cancer by intratumoral 224Radium-loaded wires is mediated by alpha particles released from atoms which spread in the tumor and can be augmented by chemotherapy," pp. 179–186, 2015.

[82] H. Park, H. Paganetti, J. Schuemann, X. Jia, and C. H. Min, "Monte carlo methods for device simulations in radiation therapy," *Physics in Medicine & Biology*, vol. 66, no. 18, p. 18TR01, 2021.

[83] X.-. M. C. Team, "Mcnp—a general n-particle transport code, version 5," 2003.

[84] I. Kawrakow, "The egsnrc code system, monte carlo simulation of electron and photon transport," *NRCC Report Pirs-701*, 2001.

[85] T. Böhlen, F. Cerutti, M. Chin, A. Fassò, A. Ferrari, P. G. Ortega, A. Mairani, P. R. Sala, G. Smirnov, and V. Vlachoudis, "The fluka code: developments and challenges for high energy and medical applications," *Nuclear data sheets*, vol. 120, pp. 211–214, 2014.

[86] F. Salvat, J. M. Fernández-Varea, J. Sempau, *et al.*, "Penelope-2008: A code system for monte carlo simulation of electron and photon transport," in *Workshop Proceedings, Barcelona, Spain*, vol. 30, 2008.

[87] IAEA, "National nuclear data center."

[88] G. Heger, A. Roy, M. Dumančić, and L. Arazi, "Alpha dose modeling in diffusing alpha-emitters radiation therapy—part i: single-seed calculations in one and two dimensions," *Medical Physics*, vol. n/a, no. n/a.

[89] U. Maucksch, R. Runge, L. Oehme, J. Kotzerke, and R. Freudenberg, "Radiotoxicity of alpha particles versus high and low energy electrons in hypoxic cancer cells," *Nuklearmedizin-NuclearMedicine*, vol. 57, no. 02, pp. 56–63, 2018.

[90] T. Cooks, M. Schmidt, H. Bittan, E. Lazarov, L. Arazi, I. Kelson, and Y. Keisari, "Local control of lung derived tumors by diffusing alpha-emitting atoms released from intratumoral wires loaded with radium-224," *International Journal of Radiation Oncology* Biology* Physics*, vol. 74, no. 3, pp. 966–973, 2009.

[91] M. Lecavalier-Barsoum, F. Khosrow-Khavar, K. Asiev, M. Popovic, T. Vuong, and S. A. Enger, "Utilization of brachytherapy in quebec, canada," *Brachytherapy*, vol. 20, no. 6, pp. 1282–1288, 2021.

[92] IAEA, "Dirac directory of radiotherapy centers."